Volume 61, issues 1–6, 12 May 2008

ISSN 0927-796X

ELSEVIER

MATERIALS SCIENCE & ENGINEERING

R

Reports: A Review Journal

Continuation of Materials Science Reports

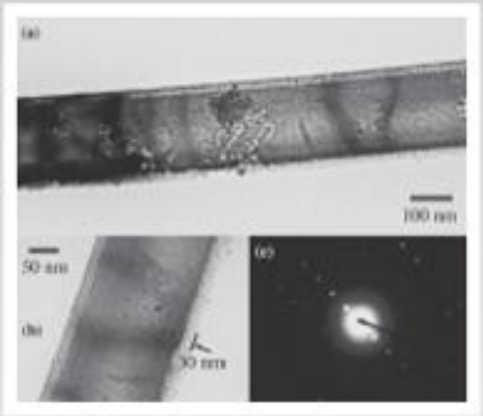

Materials Science and Engineering R 61 (2008) 59–77

Contents lists available at ScienceDirect

Materials Science and Engineering R

journal homepage: www.elsevier.com/locate/mser

Self-selective electroless plating: An approach for fabrication of functional 1D nanomaterials

Teng Qiu [a,b,*], Paul K. Chu [b,**]

[a] Department of Physics, Southeast University, Nanjing 211189, PR China
[b] Department of Physics and Materials Science, City University of Hong Kong, Tat Chee Avenue, Kowloon, PR China

ARTICLE INFO

Article history:
Available online 14 April 2008

PACS:
52.77.Dq
61.46.+w
68.37.Hk
68.70.+w
73.20.Mf
78.55.−m

Keywords:
Self-selective electroless plating
Nanowires
Dendrite

ABSTRACT

Self-selective electroless plating is a novel method to produce functional one-dimensional (1D) nanomaterials. The technique which is based on conventional electroless plating utilizes the base substrate and surface metal deposition to produce the desired functional nanostructures. Progress and advances in the past 6 years, including the production of Si nanowire arrays and concomitant noble metal dendrites by self-selective electroless plating, possible growth mechanisms, and future challenges are reviewed. The role of this approach pertaining to the future development of novel and unique nanodevices, which cannot be realized using traditional manufacturing techniques, is discussed. Intriguing recent results have shown that selective properties of the products can be obtained by controlling the electroless plating process and post surface treatment.

Contents

* Corresponding author at: Department of Physics, Southeast University, Nanjing 211189, PR China. Tel.: +86 25 52090600x8305; fax: +86 25 52090600x8204.
** Corresponding author. Tel.: +852 27887724; fax: +852 27889549.
E-mail addresses: tqiu@seu.edu.cn (T. Qiu), paul.chu@cityu.edu.hk (P.K. Chu).

0927-796X/$ – see front matter © 2008 Elsevier B.V. All rights reserved.
doi:10.1016/j.mser.2008.03.001

1. Introduction

1.1. Conventional electroless plating

Electroless plating refers to the autocatalytic or chemical reduction of aqueous metal ions and subsequent plating onto a substrate. In this process, metal ions are reduced to metals by reducing agents that are simply electron donors and the metal ions are electron acceptors which react with the electron donors. The catalyst is the sample which accelerates the electroless chemical reaction allowing oxidation of the reducing agent. In order to facilitate electron transfer, both the metal ions and reducing agent must adsorb onto the catalytic surface. The metal ions take part in the reaction in the form of charged ionic complexes. Unlike electroplating, no electrical current is required for deposition, but the substrate being plated must be catalytic in nature. A properly prepared substrate provides a catalyzed surface, and after introduction into the electroless solution, uniform deposition commences. Minute amounts of the electroless metal such as nickel, copper, etc. catalyze the reaction and so deposition is autocatalytic after the original surfaces are coated. Afterwards, electroless deposition continues, provided that the metal ions and reducing agent are replenished. However, it should be noted that the exact chemical mechanism of electroless plating is rather complicated and still remains a point of controversy.

Electroless plating is a widely used method to metallize surfaces. Using electroless plating baths, a variety of metals such as Cu, Ni, Co, Pt, Pd, Au, Ni/Co, Pb, and Sn can be deposited. The most widely used electroless plating process is electroless nickel. Electroless nickel offers unique properties including uniformity of the deposit in deep recesses, bores, and blind holes. Electroless nickel plating was first proposed by Brenner and Riddell [1,2]. Their work led to a process capable of plating the inner walls of tubes with nickel–tungsten alloy by means of an insoluble anode and brought out the unusual reducing properties of hypophosphites. In 1947, Narcus published the first paper on electroless copper plating [3], and the first commercial application of electroless copper plating was reported by Cahill in 1957 [4]. Electroless copper deposition is generally applied before electroplating on plastics and other nonconductors to provide a conductive base for subsequent plating. The electroless copper process improves the lifetime and performance in a corrosive atmosphere and upon exposure to a harsh environment. Electroless gold is currently being used in the fabrication of semiconductor devices, connector tabs, chips, and other metallized ceramics. Electroless palladium is ductile and ideal for contacts needing flexing, for instance, printed circuit board end connectors and electronic switch contacts. It has also been used as a less expensive replacement for gold to provide tarnish resistance and solderability. Similarly, thin electroless cobalt is used on magnetic memory disks and storage devices primarily for their magnetic properties.

In nanotechnologies, electroless plating is widely used in lithography and rapid prototyping. This technology allows one to produce photo masks and micro-devices with nano-size adjacent elements of different thicknesses made of various materials by conventional optical photolithography [5]. These metallic micro or nanostructures are useful in many practical applications including regular porous metal materials in photonic crystals, micro-reactors, separation filters, and so on. They have been prepared by not only top–down lithographic methods, but also bottom–up processes. The technique is simpler than other expensive and complicated methods such as electron beam or X-ray lithography and phase shift photo masking. Methods to fabricate ultra-thin, void-free, and pore-free coatings on micro, meso, and nanoparticles such as carbides, borides, nitrides, oxides, diamond, graphite, zeolites, and so on using electroless plating have also been developed. These methods also allow one to obtain nanostructured composite materials and coatings with specific properties, for instance, metal-coated fullerences, metallized carbon nanotubes, conductive nano-size additives to plastics and rubber, nanoparticle reinforced tires, sensors, detectors of chemical and biological agents, unique catalysts, adsorbents, and hydrogen storage materials.

1.2. Metal-assisted electroless etching

1.2.1. Porous semiconductors

In conventional electroless plating, the base substrate provides a catalyzed surface that is protected from etching. In 2000, Li and Bohn demonstrated a metal-assisted electroless etching method to produce light-emitting porous Si [6]. Porous Si is of interest due to their potential applications to optoelectronics. There have been three electrochemical routes to produce porous Si, namely anodic etching, photoelectrochemical etching, and laser-assisted etching, and all three processes are conducted in acidic fluoride solutions. A thin layer of Au, Pt, or Au/Pd is deposited on the Si surface prior to immersion in a solution of HF and H_2O_2. Depending on the type of metals, Si doping type (n- or p-type), and dopant concentration, porous Si with different morphologies and light-emitting properties have been produced. Studies suggest that thin metal coatings facilitate etching in HF and H_2O_2 and a reaction scheme involving local coupling of redox reactions can explain the metal-assisted etching process. This technique has been extended to the electroless fabrication of patterned nanocrystalline Si. Compared to conventional electroless plating, two different points regarding metal-assisted electroless etching should be noted. First of all, the substrate does not serve as the catalyzed surface but rather electron donors, so that it can be etched to form the nanostructured patterns.

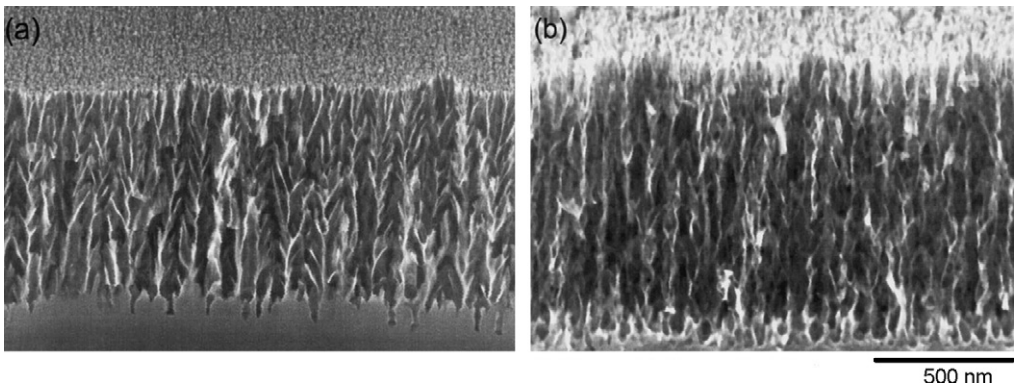

Fig. 1. Cross-sectional scanning electron microscopy (SEM) images (30° tilt) of porous GaN structures produced by Pt-assisted HF/H_2O_2 etching of n-GaN/SiC for: (a) 15 min, and (b) 40 min. The depth of the porous structure is 0.7 and 1.0 μm in (a) and (b), respectively. Reprinted with permission from ref. [7]. Copyright 2002 by American Institute of Physics.

Secondly, the metal coating is not the final product but minute amounts of the electroless metal themselves will catalyze the reaction. Hence, metal-assisted electroless etching is a novel bottom–up approach in nanotechnology. Although the actual steps are quite complex, little intervention is required on the scientist's part. The idea is to use chemistry to perform *in situ* error checking and correction that eventually guide the process toward the production of the desired structure.

The use of metal-assisted electroless etching to form other porous semiconductors has been pursued further by Bohn and co-workers. The large surface area, band gap shift, and efficient luminescence bode well for applications of porous semiconductors in chemical and biochemical sensing. Production of nanoporous GaN structures by metal-assisted electroless etching from epitaxial GaN on SiC substrate has been reported [7]. Interests in porous GaN arise from the potential of blue-shifting the band gap further into the ultraviolet region in addition to the enhanced thermal, mechanical, and chemical stability. It also serves as a buffer layer to template epitaxial growth of GaN with low strain and dislocation density. The resulting porous GaN structure exhibits cathodoluminescence with two blue-shifted bands. Appearance of the blue-shifted emission is correlated with the development of highly anisotropic wire-like structures as shown in Fig. 1 and the higher energy cathodoluminescence band originates from the portion of the structure with the smallest feature size. The experimental results suggest that the blue-shifted emission arises from quantum confinement effects. Production of porous SiC produced using metal-assisted electroless etching has also been reported [8]. In the experiments, platinum metal deposited on the wafer before etching serves as the catalyst for reduction of the chemical oxidant. The etchant is composed of aqueous HF and $K_2S_2O_8$. Various porous morphologies which depend on the etchant concentration, etching time, and SiC polytype have been observed.

Although porous semiconductors are still typically produced by anodic etching in which the semiconductor being biased positively in a conductive electrolyte facilitates oxidation and removal of surface atoms, metal-assisted electroless etching is gaining ground as the fabrication technique because of its simplicity and ability to etch objects with irregular shape thereby offering advantages in the synthesis of porous semiconductors. However, the mechanism of electroless plating is still unclear. For example, the films produced by metal-assisted etching typically have a different structure compared to that of conventional porous semiconductors. One of the questions is that whether morphological control can be further enhanced to form the desired nanostructures. A better understanding of the mechanism and physical principle is required to better control the structure and properties of the films.

1.2.2. Nanoholes in Si

Although the formation of metal-induced patterns during electrochemical copper deposition in a diluted hydrofluoric acid solution has been reported by Morinaga et al. [9], Kim et al. [10], and Mitsugi and Nagai [11], the use of controlled metal-assisted electroless etching to form the designed nanopatterns has only been reported recently by Tsujino and Matsumura [12,13]. In their experiments [13], Ag particles were deposited on the surface of a p-type Si(1 0 0) wafer by electroless plating. The size of the particles ranged from 30 to 100 nm. The wafers with the Ag nanoparticles were immersed in a solution containing HF and H_2O_2 and the wafer was covered by a 300 nm thick microporous layer (Fig. 2(a)). As shown in Fig. 2(b), straight lines normal to the surface and short lines parallel to the surface under the microporous Si layer can be seen. The structure extends to a depth of about 5 μm from the surface. At a distance of about 40 μm from the surface as illustrated in Fig. 2(c) and (d), straight cylindrical holes are present. Ag particles with a diameter similar to that of the pore are found on the bottom of these holes. If the etching time is extended to 10 h, pores as deep as 500 μm and ~50 nm in diameter can be obtained. What differentiates Pd and Cu from Ag is that helical pores exist below the microporous region [12]. The helical macropores are also observed in Ag sometimes. The cylindrical pores can be changed to helical ones by altering the solution concentrations and the walls of the macropores are lined with the microporous Si. The formation mechanism of the nanoholes is rather complicated. It is speculated that the unique catalytic property of the Ag particles enables the formation of the cylindrical holes due to the strong catalytic activity of Ag to decompose hydrogen peroxide and produce AgO_x on the surface. Since the oxide is a strong oxidant, the Si wafer is oxidized by AgO_x at the Si/Ag interface and the nanoholes result from dissolution of the silicon oxide by HF.

Owing to their potential applications in photonic crystals [14], micromachining [15], and so on, nanoholes in Si have been investigated further by others. Cruz et al. [16] have observed the formation of some straight macropores together with the presence of interconnecting lateral pores produced in a HF/H_2O_2/CH_3CH_2OH solution with Au or Pt particles. The etching depth is proportional to the etching time up to 3 h, at which time it stops. Increased temperature (40 °C versus room temperature) has also been observed to increase the etching rate.

1.3. Self-selective electroless plating

When thin metal coatings or particles are deposited on the surface of semiconductor wafers followed by etching in HF and H_2O_2, gas evolution from the metal-coated area, especially Pt and Au/Pd, ensues due to the absence of metal dissolution. Hole

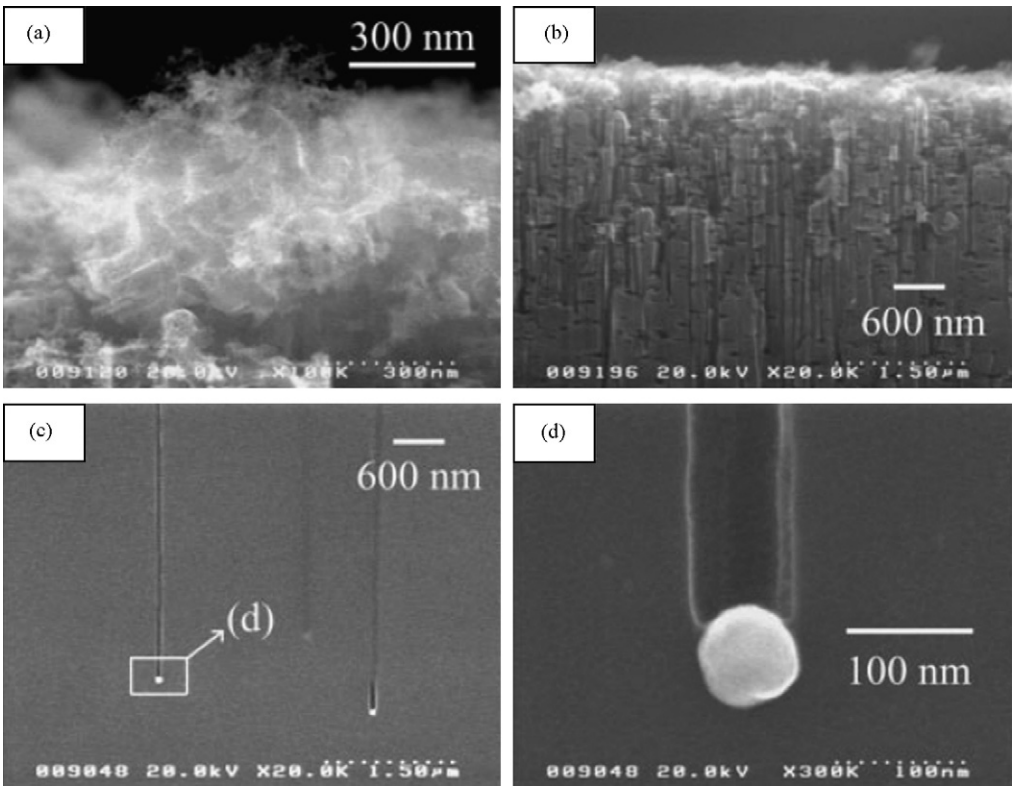

Fig. 2. Cross-sectional views of a p-type Si(1 0 0) wafer loaded with Ag particles after etching for 30 min: (a) in a region of the microporous Si layer (about 300 nm from the surface), (b) in a region about 3 μm from the surface, (c) at a position about 40 μm from the surface, and (d) magnified view of the bottom of the hole shown in (c). Reprinted with permission from ref. [13]. Copyright 2005 by WILEY-VCH Verlag GmbH & Co. KGaA, Weinheim.

injection is provided by the reaction of H_2O_2 on the metal particles. The holes are injected into the semiconductor valence band and then diffuse away from the metal particles explaining why etching is confined to the near-particle area. The dissolved O_2 also plays the role of an oxidant but only leads to etching with a very small rate [17].

Metal-assisted electroless etching is used to produce the desired nanostructures on the base substrate but does not play a major role in metal deposition. This is in contrast with conventional electroless plating which employs surface metallizing. Researchers have recently found that when conducting HF/$AgNO_3$ etching on Si, aligned Si nanowire (SiNW) arrays and dendrite-like silver coatings can be obtained on the surface [18]. These two nanostructures have subsequently been demonstrated to have potential applications in nanoscale electronics and photonics. Based on the preliminary formation mechanisms and the relationship with conventional electroless plating, the new technique is termed self-selective electroless plating in which the desired functional nanostructures are produced on both the substrate and deposited metal.

In this review, recent advances in the production of nanostructures by self-selective electroless plating (primarily in the past 6 years), growth mechanisms, and future challenges are described. Recent results have shown that selective material properties can be accomplished by controlling the electroless plating process and post surface treatment. It is believed that self-selected electroless plating will play a more important role in the fabrication of future nanoelectronic and optoelectronic devices.

2. Self-selective electroless plating on Si

2.1. Possible growth mechanisms of Si nanowire arrays

Metal-assisted electroless etching has been conducted on Si to form porous Si and Si nanopores. In the redox reaction in which both the anodic and cathodic processes occur simultaneously on

Table 1
Description of the final product morphologies produced by self-selective electroless plating on Si using different etching parameters (adapted from refs. [18,23,24,83]

Etching parameters (etching time is 60 min in all cases)	Morphologies of the base Si substrate	Morphologies of the metal coatings
0.02 mol/L $AgNO_3$ and 5.0 mol/L HF at 50 °C	Free-standing SiNW arrays	Silver dendrites
0.01 mol/L $KAuCl_4$ and 12 mol/L HF at 50 °C	Free-standing SiNW arrays	Gold dendrites
0.015 mol/L $AgNO_3$ and 5.0 mol/L HF at 50 °C	Regular porous Si microstructures	Silver dendrites
0.02 mol/L $AgNO_3$ and 5.0 mol/L HF at 15 °C	Large-area micrometer-sized stalagmitic structures	Silver dendrites
0.02 mol/L $AgNO_3$ and 5.0 mol/L HF at 120 °C	Disordered porous structures	Silver dendrites
0.02 mol/L $AgNO_3$ and 5.0 mol/L NH_4F at 50 °C	No pits	Micrometer-sized silver grain film
0.02 mol/L $KAuCl_4$ and 5.0 mol/L HF at 50 °C	Disordered shallow pits	Gold nanowhiskers
0.08 mol/L $Ni(NO_3)_2$ and 10 mol/L HF at 140 °C	Large quantities of pillar-like structures	No metal deposition
0.15 mol/L $Ni(NO_3)_2$ and 10 mol/L HF at 140 °C	Crater-pit-like microstructures	No metal deposition
0.02 mol/L $Cu(NO_3)_2$ or K_2PtCl_6 with 5.0 mol/L HF at 50 °C	Disordered shallow pits	Continues metal grain films
$Mn(NO_3)_2$, $Fe(NO_3)_3$, $Co(NO_3)_2$, $Cr(NO_3)_2$, or $Mg(NO_3)_2$ with 12 mol/L HF at 140 °C	The micrometer-sized pillar-like, cone-like, or crater-pit-like microstructures	No metal deposition

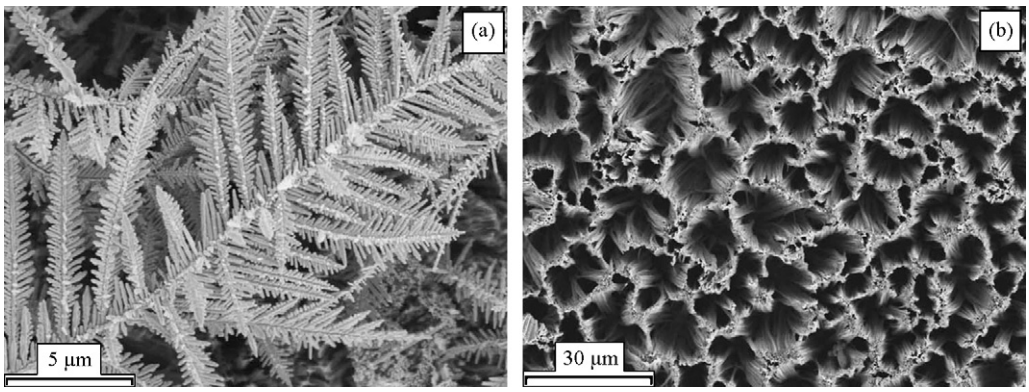

Fig. 3. SEM images of silver and etched silicon prepared in 0.01 mol/L $AgNO_3$ and 4.6 mol/L HF at 50 °C for 60 min: (a) silver dendrites and (b) surface morphology of etched silicon showing SiNW arrays. Reprinted with permission from ref. [24]. Copyright 2004 by Elsevier.

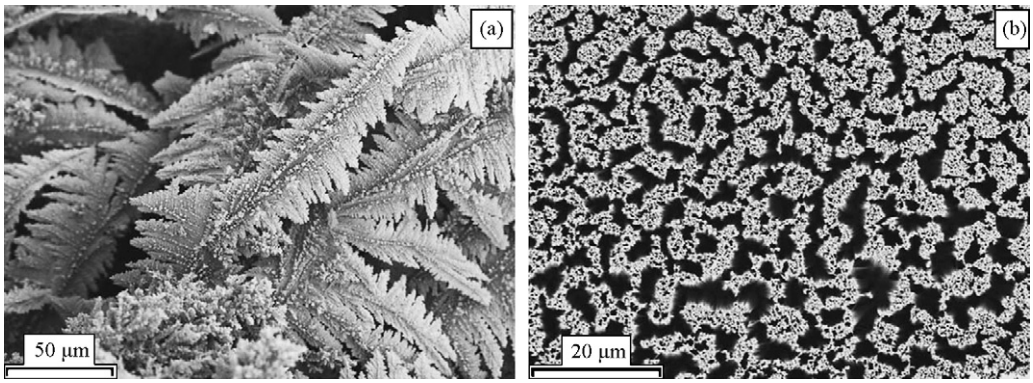

Fig. 4. SEM images of gold and etched silicon prepared in 0.01 mol/L $KAuCl_4$ and 12 mol/L HF at 50 °C for 60 min: (a) gold dendrites and (b) surface morphology of etched silicon showing SiNW arrays. Reprinted with permission from ref. [24]. Copyright 2004 by Elsevier.

the Si surface, charge exchange occurs via the substrate [19–22]. Peng and co-workers [18,23] have subsequently prepared large-area silicon nanowire (SiNW) arrays on Si wafers in an aqueous HF solution containing $AgNO_3$ or $KAuCl_4$ at a low temperature using self-selective electroless plating. The morphologies of the obtained structures are strongly affected by the etching parameters such as the etching temperature, solution concentration, and also the metal species added to the HF solution, as illustrated in Table 1. Based on the experimental results, it can be concluded that dendrite-like metal coatings (silver and gold dendrites shown in Figs. 3(a) and 4(a)) play a critical role in the formation of SiNW arrays shown in Figs. 3(b) and 4(b) [24].

2.1.1. Preliminary mechanism I: Protection of silicon from etching by surface Ag

Electroless plating is based on the galvanic displacement reaction in which cathodic reaction and anodic reaction occur simultaneously. In the Si–$AgNO_3$–HF system, the holes injected from the silver ions are consumed by an oxidation process and deposition can occur without an externally applied bias. The possible mechanisms are described in the following [25].

(1) The injected holes are consumed by oxidation on the silicon surface and the substrate atoms are replaced by silver atoms (displacement plating).
(2) The holes injected during silver deposition are transferred to an electron donor in the solution.
(3) The silver ion and reducing agent in the solution react directly at the catalytic sites on the surface without involving the substrate in the charge transfer process.

In the first case, the oxidation products must be soluble in the solution in order to prevent the formation of a passivating layer. This is possible on Si because SiO_2 is soluble in a low-pH HF solution. In principle, the thickness of the silver film is limited since the deposition process cannot continue after complete coverage is achieved. The morphology and adhesion of the deposit may be

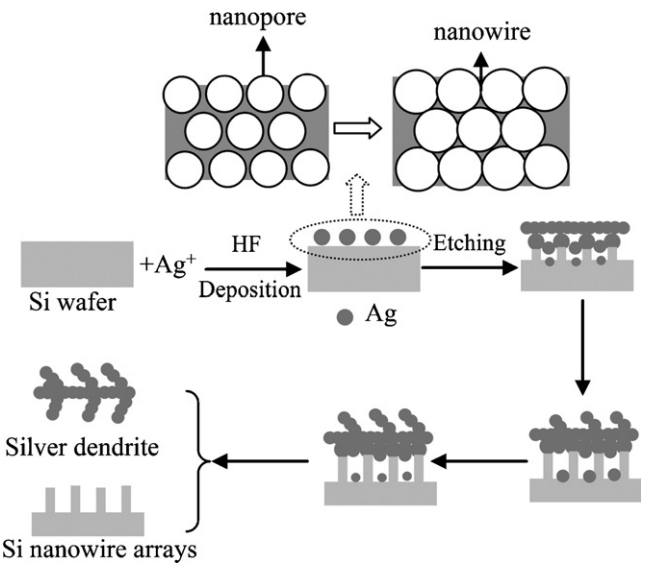

Fig. 5. Schematic illustration of the growth process of the SiNW arrays and silver dendrites. Reprinted with permission from ref. [25]. Copyright 2006 by TMS.

poor due to simultaneous dissolution of silicon and deposition of silver. The second case is not frequently encountered in the deposition of metals on semiconductors since the rate of transfer of holes to the solution is usually slower than the trapping of holes by surface atoms, which is the first step in the oxidation mechanism. This situation is similar to the stabilization of semiconductor surfaces under illumination in photoelectrochemical energy conversion [26]. The third case is often exploited in electroless deposition of metals on semiconductors. For instance, small clusters of palladium or other metals are deposited by the displacement mechanism and then they act as the catalytic sites for the reduction of metal ions and oxidation of the reducing agent in the solution.

Based on these considerations, the possible mechanism of self-selective electroless plating of SiNW arrays can be deduced (see Fig. 5) [18,23–25,27]. In the beginning, Si etching and silver/gold deposition occur simultaneously on the Si surface. The deposited silver/gold atoms form nuclei on the surface of the Si substrate and hence, many silver/gold nanoclusters are uniformly distributed on the surface of Si substrate initially. These nanoclusters and the areas surrounding these nuclei act as, respectively, the local cathodes and anodes in the electrochemical redox reaction. That is to say, many nano-size free-standing electrolytic cells can assemble spontaneously on the Si surface in the aqueous HF solution. Generally, these metal nanoclusters have strong tendency to coalesce and form a continuous film during electroless plating. Coalescence is more favorable than the metal coating in industrial applications, but simultaneously, it will lead to the disappearance of free-standing electrolytic cells and uniform etching of Si substrate. Electroless plating of Pt and Cu in HF can normally be categorized in this way. If HF is substituted by NH_4F, the silver deposits also coalesce strongly and produce a continuous film that adheres well to the Si substrate. However, in the HF–$AgNO_3$ and HF–$KAuCl_4$ system, the simultaneous growth of silver/gold dendrites effectively deters coalescence of the nanoclusters by consuming large quantities of superfluous deposited atoms, and so these free-standing nanoscale electrolytic cells are preserved. The nanoscale electrolytic cells lead to selective etching of the Si

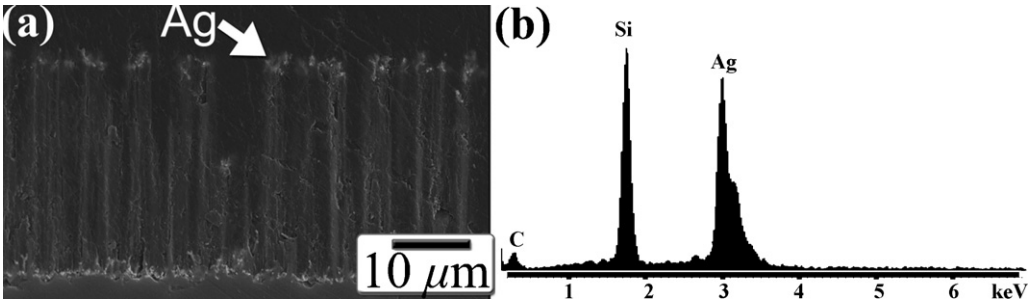

Fig. 6. (a) Cross-sectional SEM image of the Ag capped SiNW arrays. (b) EDS spectrum of the as-grown Ag capped SiNW arrays. Reprinted with permission from ref. [28]. Copyright 2006 by IOP Publishing Ltd.

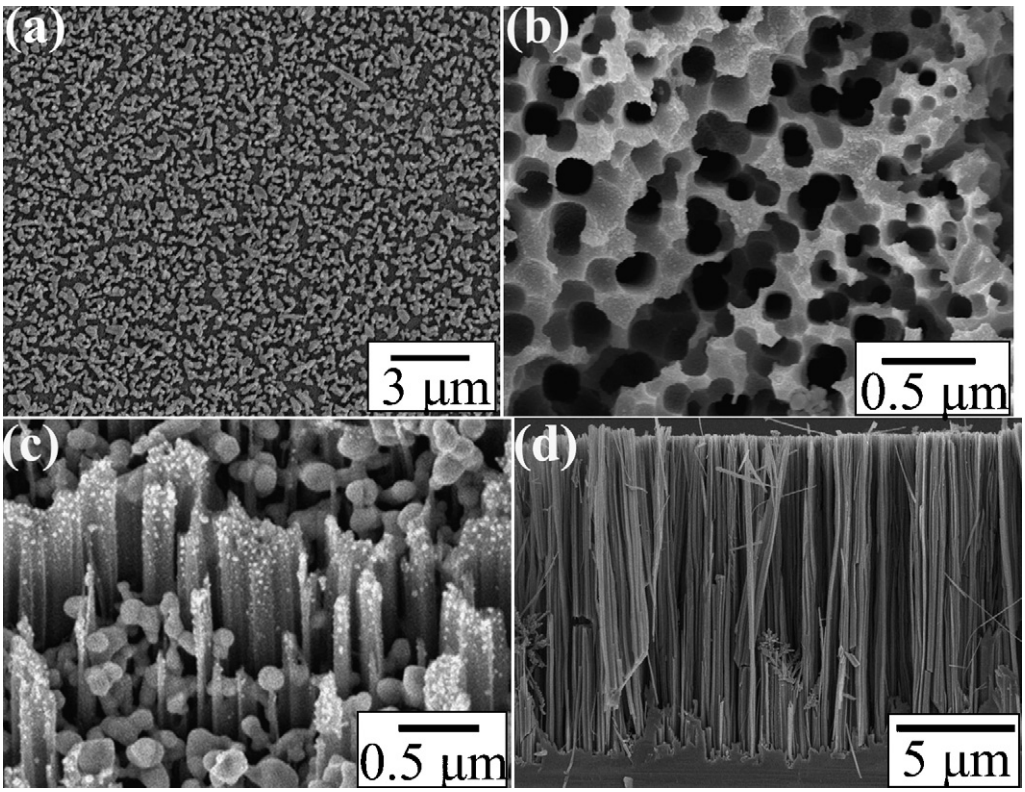

Fig. 7. SEM images of: (a) silver nanoclusters distributed on the Si wafer at the initial stage, (b) nanopores at the intermediate stage, and (c) surface morphology of the Si wafer etched for 10 min, showing silver nanoclusters embedded in the SiNW arrays and tiny silver nanocrystals attached on the apexes and walls of the SiNWs, and (d) cross-sectional SEM image of SiNWs formed during 60 min etching in the end. Reprinted with permission from ref. [30]. Copyright 2006 by American Vacuum Society.

substrate followed by silver/gold deposition and the anodes are etched while the cathodes are preserved. As a result, Si nanowires (SiNWs) capped with silver nanoclusters acting as the cathode are eventually formed at the expense of etching of the surrounding Si acting as the anode. Fig. 6 depicts the cross-sectional SEM image of the as-grown Ag capped SiNWs obtained by using a solidified agent to affix the sample for improved contrast [28]. The white spots on the tips of the SiNWs in Fig. 6(b) are silver nanoclusters. The main constituents are confirmed to be Ag and Si by energy dispersive X-ray (EDS) spectroscopy.

The growth mechanism has been further studied by analyzing the intermediate nanostructures [29,30]. Fig. 7 depicts the SEM micrograph of Si which has undergone self-selective electroless plating in HF–$AgNO_3$ [30]. Fig. 7(b) reveals that the intermediate holes on the surface of silicon are important to the formation of the SiNWs. As shown in Fig. 5, the deposited silver atoms first form nuclei and then nanoclusters which are uniformly distributed on the surface of the silicon wafer. Small flat honeycombs form around the tiny deposited silver nanoclusters. Therefore, there are many nano-sized honeycomb-like anodes surrounding the silver nanoclusters which act as the local cathode forming an electrochemical cell. These cells self-assemble on the surface of the silicon wafer. The honeycombs around the silver nanoclusters become larger and deeper via the etching action and many of them aggregate to form one nanopore. If the silicon wall between two nanopores has not yet been etched completely, that is, the nanopore boundary still consists of a thin silicon wall, as shown in Fig. 7(b), an undetached Si nanotube forms. Further etching of the intermediate undetached Si nanotubes leads to the formation of SiNWs with a special shape. Fig. 7(c) displays the SEM image of the as-grown SiNWs. The damaged tube walls (thin layers) are attached to the nanowires, indicating that they are the residual walls at the triple points between the cell grains. The residual tube walls give rise to large SiNW diameters of 30–300 nm as shown in the SEM images.

2.1.2. Preliminary mechanism II: Catalysis of Si etching by Ag particles in contact

In addition to the mechanism stipulating that Ag protects the silicon underneath from etching, a different mechanism with some supporting evidence has been stipulated. Some researchers have different opinions about where oxidation and dissolution of Si substrate occur during self-selective electroless Ag plating [31,32]. It is claimed that oxidation and dissolution of Si do not occur alongside the Ag deposits, but rather beneath them as shown in Fig. 8 [31]. The alternative mechanism is as follows. In the initial stage of silver deposition, Ag^+ ions in the vicinity of the silicon surface capture electrons from the valence band of Si and are subsequently deposited in the form of metallic Ag nuclei on a nano-scale. As the Ag nuclei are more electronegative than Si, they attract electrons from Si and become negatively charged. These Ag nuclei serve to catalyze subsequent reduction of Ag ions and facilitate Si oxidation. Therefore, other Ag^+ ions near the Si surface get electrons preferentially from the Ag nuclei and are deposited around them. The Ag nuclei grow to larger particles as more Ag ions are deposited. Meanwhile, because Si beneath the Ag particles provides electrons to reduce the Ag ions, excess local oxidation occurs and SiO_2 is produced under these Ag nanoparticles. Shallow pits form below the Ag nanoparticles due to the etching of SiO_2 by HF and then the Ag particles enter the pits.

With regard to experimental verification of this proposed mechanism, Morinaga et al. and Kim et al. have reported that electrochemical Cu deposition accompanies local oxidation and dissolution of silicon. It takes place under the deposited Cu inducing the formation of pits at the same location as a result of etching in HF [9,10]. Mitsugi and Nagai have also reported pit

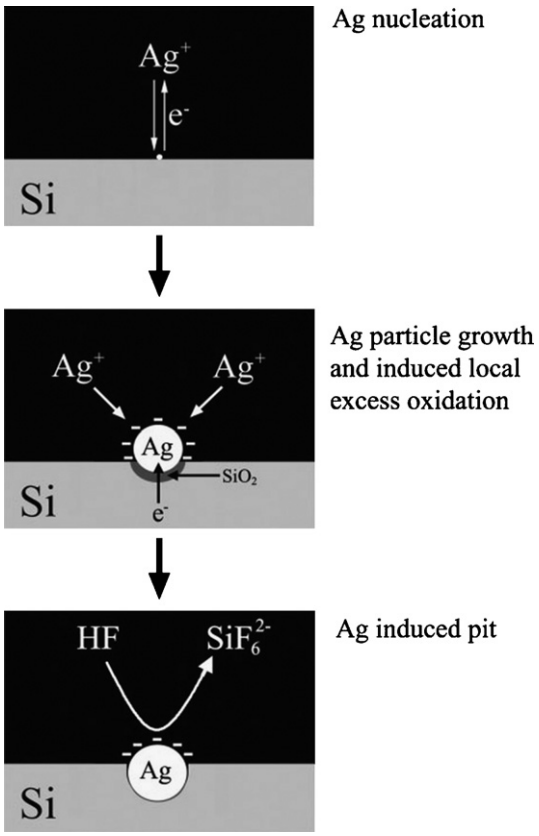

Fig. 8. Mechanism of electroless Ag deposition on a Si substrate in HF/$AgNO_3$ solution. Reprinted with permission from ref. [31]. Copyright 2006 by WILEY-VCH Verlag GmbH & Co. KGaA, Weinheim.

formation caused by Cu contamination in a diluted HF solution [11]. They propose that the local redox couple between Cu and the nearby Si surface is essential to the formation of the local pits which are formed at the same place as the Cu islands. Tsujino and Matsumura have further demonstrated controlled metal-assisted electroless etching to form the designed nanoholes in silicon as discussed in Section 1.2.2 [12,13].

Based on these observations, the growth mechanism of SiNWs and dendrites in self-selective electroless plating is postulated in the following (see Fig. 9) [32]. At first, shallow pits containing the Ag particles form due to etching of the produced SiO_2. As the reaction proceeds, some small Ag particles sink into the deep pits, but large Ag particles that cannot enter the pits grow into large, branched silver dendrites that eventually cover the entire surface of the Si wafer [Fig. 9(C)]. Subsequent deposition of Ag occurs on these silver dendrites and the growth consumes a large quantity of superfluous silver atoms. This effectively prevents the formation of a compact Ag granular film and also the growth of small Ag particles trapped in the pits. Because the Ag particles are trapped by the pits and cannot move horizontally on the silicon surface, highly localized and site-specific etching occurs beneath these trapped Ag particles. Under these circumstances, the initial shallow pits deepen as the underlying SiO_2 dissolves and the Ag particles sink further. Therefore, straight, non-interacting cylindrical pores orthogonal to the Si surface form eventually (Fig. 9(E)). The pore size and separation distance depend upon the size and areal density of the trapped Ag particles located at the bottom of the deep pores. Subsequent chemical dissolution of the thin pore walls enlarges the pores leading to merging of adjacent pores. Finally, after sufficient etching, large quantities of one-dimensional SiNWs are formed on the silicon surface (Fig. 9(F)).

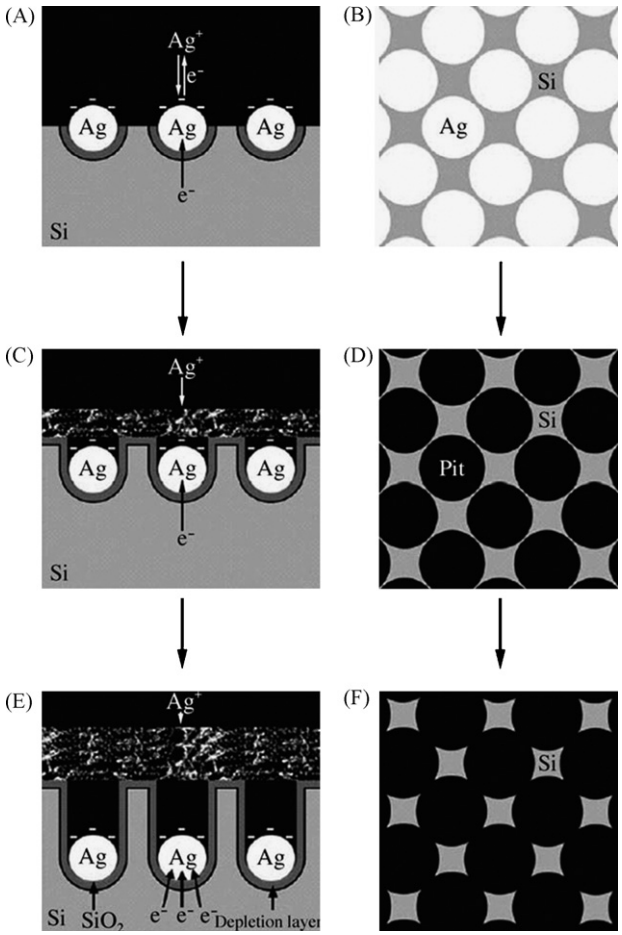

Fig. 9. Schematic representation of the formation of vertically aligned SiNW arrays on the Si surface in aqueous HF/$AgNO_3$ solution. (A, C, E) The lateral view of the etching process and (B, D, F) the top view of etching process. Reprinted with permission from ref. [32]. Copyright 2006 by WILEY-VCH Verlag GmbH & Co. KGaA, Weinheim.

2.1.3. Preliminary mechanism III: Formation of perpendicular Si nanowire arrays due to the synergistic effects of the intrinsic catalytic properties of Ag as well as the Ag cluster network

Because it is quite difficult to determine the change in the exact location of a single particle during self-selective electroless plating and dynamic progress combining *in situ* HF chemical etching of SiNWs and observation by transmission electron microscopy (TEM) or scanning electron microscopy (SEM), the role of the Ag particles and the exact mechanism of formation of SiNWs and dendrites in self-selective electroless plating remain controversial. Fang, et al. have recently performed dry self-selective electroless plating and observed that Ag catalyzes etching of silicon beneath the silver in both the random downward and vertical directions [33]. They believe that in the net-like Ag nanocluster structure, the interaction among clusters reduces the ability of each cluster to move freely, resulting in the collective sinking of the Ag nanoclusters vertically downwards. Consequently, the morphology of the Si nanostructures changes from an irregular shape in the early stage of etching to a regular shape after etching. The schematic diagram illustrating the possible formation process of the SiNW arrays on the Ag dry-deposited Si substrate is displayed in Fig. 10. After thermal deposition on the silicon wafer (Fig. 10(a)), most of the Ag clusters form an island-like network on the silicon substrate. During the etching process, the silicon underneath the Ag clusters acts as the anode and is locally oxidized into SiO_2, followed by immediate dissolution of SiO_2 by HF resulting in the formation of shallow pits under the Ag clusters. The Ag clusters which serve as the cathode to transport the electrons released from Si to facilitate Si oxidation gradually sink into the etched pits. In the initial etching stage (Fig. 10(b)), collective sinking of the Ag clusters scratches the Si surface, in conjunction with breaking up of some big clusters into small clusters or particles, gives rise to the formation of porous silicon. The clusters possibly do not sink vertically downwards because a stable structure and balanced network have not yet formed. Subsequent dissolution of the thin pit wall leads to the formation of free-standing silicon nanostructures (Fig. 10(c)). When the stable Ag nanoparticle network forms, interaction among clusters causes the structure to sink vertically leading to the formation of SiNW arrays vertical to the substrate surface (Fig. 10(d)). The etching product, that is, vertical SiNW arrays containing the Ag nanocluster mesh, can be considered a secondary catalyst to other specific catalytic reactions, as illustrated in Fig. 11. The EDS maps in Fig. 11(d) and (e) disclose the distributions of Ag and Si which are consistent with their morphology displayed in Fig. 11(c). Thus, the SiNWs are surrounded by a network of Ag clusters and the space in between the SiNWs is thought to be the sinking paths for the Ag clusters.

The growth mechanism is not applicable to self-selected electroless Au plating in which large area SiNW arrays can also be formed. In similar experiments involving evaporation of Au films with different thicknesses on silicon wafers before etching, only irregular etching results, instead of SiNW arrays, are obtained. The reason may be the poor wettability of Au on the native thin SiO_2 layer on the silicon substrate. It may affect the contact between the Au and substrate and consequently the catalytic properties of the Au clusters [34]. Another possible reason is that some reactions may take place between Au and Si. The Au clusters drop onto the wafer surface via thermal evaporation and at the moment they come into contact with wafer, the instant temperature locally may be higher than the lower eutectic point of Au–Si (363 °C in bulk) [35]. Some clusters may react with the Si substrate changing their catalytic properties.

It should be mentioned that all three proposed mechanisms are not supported by sufficient convincing experimental evidence. Quoting Fang et al. [33], the wet deposition procedure introduces difficulty in detecting the exact change in the position of a single

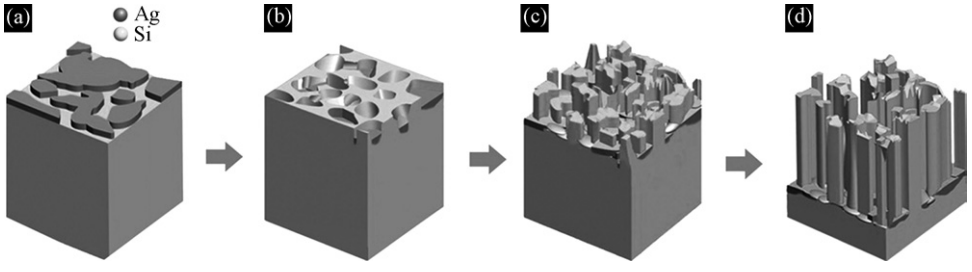

Fig. 10. Schematic diagram of the possible formation process of SiNW arrays on an Ag dry-deposited Si substrate in H_2O_2/HF solution. Reprinted with permission from ref. [33]. Copyright 2006 by IOP Publishing Ltd.

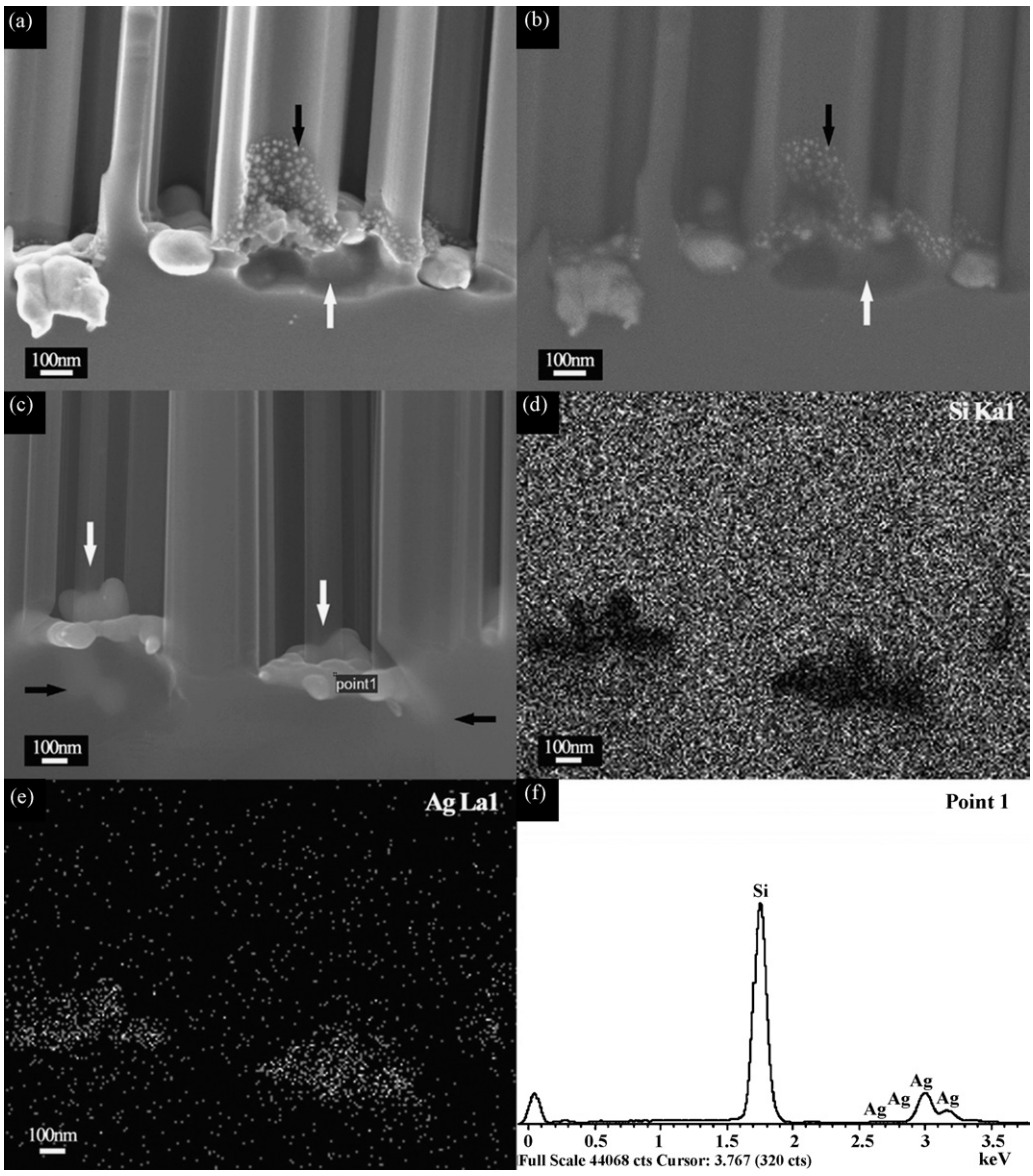

Fig. 11. Cross-sectional view of the bottom of SiNWs for a longer etching time: (a) secondary electron image (SEM accelerating voltage = 5.0 kV), (b) back-scattering electron image corresponding to (a), (c) secondary electron image (SEM accelerating voltage = 15 kV), (d) EDS mapping result of Si Kα1 corresponding to (c), (e) EDS mapping result of Ag Lα1 corresponding to (c), (f) EDS point analysis of Ag clusters at the bottom of the SiNWs in (c). Reprinted with permission from ref. [33]. Copyright 2006 by IOP Publishing Ltd.

particle during etching and in the formation of the three-dimensional disordered stacked Ag particle structure during deposition. Furthermore, it is hard to monitor in details the dynamic progress of wet catalytic etching, which is still hitherto unclear. It is compounded by the difficulty in combining *in situ* HF chemical etching of SiNWs with observation by TEM or SEM. According to Fang's experiment, it is still unclear what exactly causes the changes, for example, why some Ag clusters become slightly smaller during etching, why some small particles are separated from the big clusters, and why these changes lead to morphological change in the Si nanostructures from an irregular shape at the early stage of etching to a regular shape after etching. Hence, more analysis is necessary in order to elucidate the exact mechanism.

2.2. Growth mechanism of dendrites

A dendrite-like metal coating plays an important role in the formation of SiNW arrays in self-selective electroless plating on Si. Formation of the silver/gold dendrites should be considered within

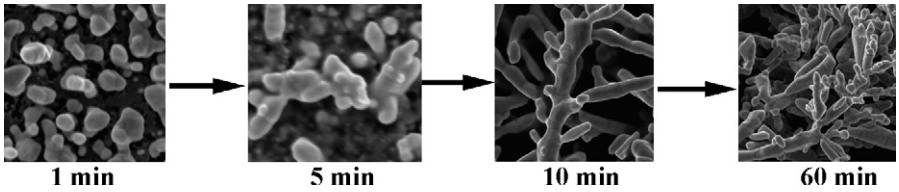

Fig. 12. Growth-time dependent morphologies of the silver structures demonstrating the diffusion-limited aggregation process (growth time = 1 min, 5 min, 10 min, and 60 min).

the framework of a diffusion-limited aggregation model [36,37] that involves cluster formation by adhesion of a particle via a random path to a selected seed and particle diffusion to stick to the growing structure as shown in Fig. 12. The *in situ* prepared honeycombs around the silver nanoclusters can be regarded as the template similar to that reported in Xiao's work about ultrasonically assisted template synthesis of palladium and silver dendritic nanostructures [38]. In the initial stage, high concentrations of the silver salt and reduction agent lead to reduction–nucleation–growth of the silver/gold nanoclusters on multiple locations to form a chain-like network. As the reaction continues, the concentrations of the silver/gold salt and reduction agent decrease appreciably, and the growth is mainly driven by the reduced surface energy thereby resulting in the formation of the dendritic silver/gold nanostructures.

2.3. Properties and applications of Si nanowire arrays

Based on the vapor–liquid–solid growth mechanism, various techniques have been developed to fabricate SiNWs and they mainly include physical deposition, laser ablation, evaporation, and solution methods. However, high temperature, hazardous silicon precursors, complex equipment, and other rigorous conditions are often required. Moreover, these often complicated routes typically yield disordered entanglements of nanowires hampering subsequent experimental characterization and potential applications. It is known that the axial crystallographic orientations of 1D silicon nanostructures are expected to influence their electronic structure (energy gap) as well as their physical properties (electron transport) according to previous theoretical calculations. Hence, the accurately controlled fabrication of ordered SiNW arrays with the desirable axial crystallographic orientation using simpler and quicker ways is very desirable and of great importance to materials synthesis and future nanoscale optoelectronic devices that employ silicon. In this respect, the technique of self-selective electroless plating can produce single-crystal high-quality SiNW arrays with the desirable crystallographic orientation readily and controllably by selecting silicon wafers with the corresponding crystallographic orientation [39].

2.3.1. High antireflection property

It has been reported that SiNW arrays fabricated on either monocrystalline or polycrystalline Si substrates using self-selective electroless plating can diminish reflection drastically over a wide spectral bandwidth from 300 to 1000 nm [39,40]. The reflectance from the arrays on single crystalline Si is about 1.4% and much less in the range of 300–600 nm. It is believed that this remarkable property arise from the high density of the 1D silicon nanostructures, because the sub-wavelength structured surface can suppress reflection over a wide spectral bandwidth and a large field of view, in addition to the introduction of a possible porosity gradient throughout the SiNW arrays.

2.3.2. Photovoltaic application

The optical antireflection behavior of the SiNW arrays closely resembles that of a multi-antireflection coating and bodes well for applications to high-efficiency Si solar cells [41–44]. Peng and coworkers have investigated SiNWs from the perspective of photovoltaic applications [40]. The processing sequence consists of the following steps: (i) formation of oriented SiNW arrays on p-type silicon using self-selective electroless plating, (ii) chemical cleaning to remove the remaining Ag and other contaminants adhered to the SiNW arrays, (iii) p–n junction preparation by $POCl_3$ diffusion, (iv) vacuum evaporation of metallic aluminum onto the rear surface and sintering at 800 °C to remove the parasitic p–n junction at the backside, (v) vacuum evaporation of metallic silver onto the rear surface and masked evaporation of a Ti/Pd/Ag front grid onto the surface of the SiNW arrays functioning as both the emitter and antireflection coating. However, the photovoltaic conversion efficiency is not as high as that expected of the excellent antireflecting properties. In order to improve the important photovoltaic parameters such as short-circuit current and open-circuit voltage, phosphorus diffusion and fabrication of contacts need to be optimized. Consequently, in spite of the potential, the efficiency of these nanowire-based photovoltaic cells prepared by self-selective electroless plating needs further improvement and investigation.

2.3.3. Ultraviolet emission property

The SiNW arrays with Ag caps have also been observed to exhibit strong ultraviolet emission with the peak at 330 nm [27]. The intensity of the peak varies nonlinearly with annealing temperature and time, but its position remains unchanged. Analysis of the emission and excitation spectra suggests that the ultraviolet emission is closely related to the existence of silver vacancy defects in the silver nanocaps formed during sample fabrication [45]. The bonding states of Si and Ag at the interface of the Ag caps and SiNWs have been studied. Sun et al. have observed that Ag can readily terminate the surface dangling bonds, replacing less stable Si–H bonds, and form more stable Si–Ag bonds [46]. The Si–Ag bonds are also expected to passivate the sample surface. Moreover, stable Si–Ag bonds can suppress formation of Si

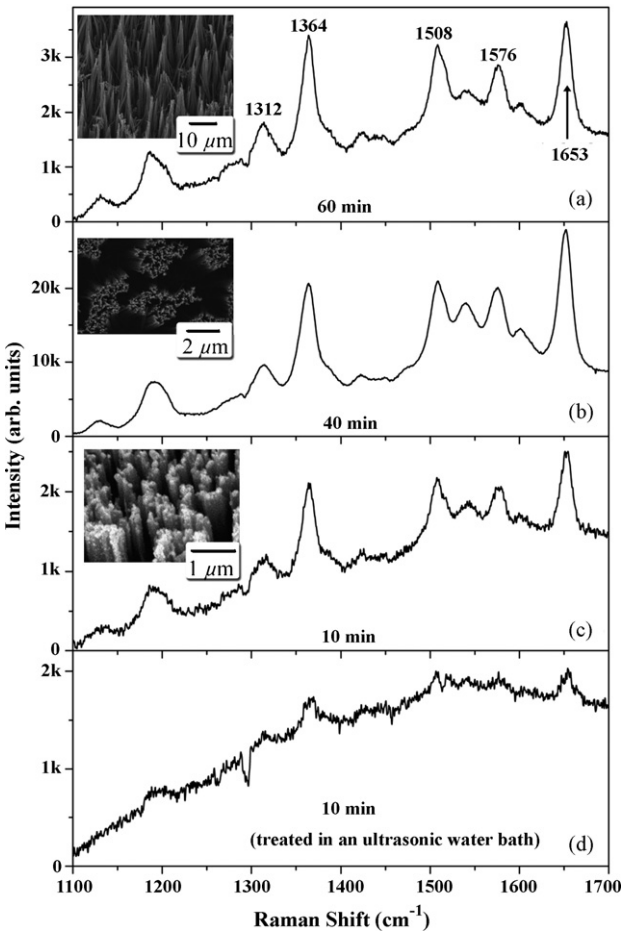

Fig. 13. SERS spectra acquired from rhodamine 6G adsorbed on the Ag capped SiNW arrays etched for different times: (a) 60 min, (b) 40 min, and (c) 10 min. The insets show the corresponding morphologies of the samples, respectively. For comparison, the Ag capped SiNW arrays shown in the inset of Fig. 13(c) are treated in an ultrasonic water bath for 10 s to remove the Ag caps and Fig. 13(d) shows the reduced Raman signals from this sample. Reprinted with permission from ref. [28]. Copyright 2006 by IOP Publishing Ltd.

dangling bonds giving rise to more intense and stable visible luminescence from the etched silicon nanocrystals due to the quantum confinement effect [47–49].

2.3.4. Raman spectroscopy and field electron emission properties

Raman spectra acquired from the SiNW arrays after the Ag cap has been removed show a downshift and asymmetric broadening due to the phonon quantum confinement effects as well as intensity enhancement [50–54]. Field electron emission from the SiNWs has also been investigated [50]. The turn-on field is about 12 V/μm at a current density of 0.01 mA/cm^2. These highly densified and ordered SiNW arrays are expected to have potential applications in vacuum electronic or optoelectronic devices.

2.3.5. Surface-enhanced Raman characteristics

The gaps between Ag caps on individual SiNWs can be controlled by varying the etching time during self-selective electroless plating [25,28]. The longer SiNWs produced by etching for a longer time such as 40 or 60 min are not as rigid as those produced by etching for 10 min. Bending of the nanowires leads to large Ag caps that can sometimes be bundled together as shown in the inset in Fig. 13(b). This phenomenon can be explained by the irregularity of the individual nanowires [29]. The center of gravity of each individual nanowire is not aligned and the longer nanowires off axis to gravitation tend to bend more and eventually, the torque leads to more bending and agglomeration of the nanowires. Van der Waals attraction among the atoms may also play a role.

Lee et al. have proposed a simple method to obtain high surface-enhanced Raman scattering (SERS) [55]. In their technique, the analyte molecules spontaneously occupy the space between adjacent tips of the Ag nanowires that are produced in porous aluminum oxide by controlled dissolution of the alumina matrix. Although the protocol is quite innovative from the perspective of fabrication of hot geometries, the tips of the nanowires can bend towards each other and so there is room for optimization. Moreover, the hot geometry produced has the "tip/analyte/tip" arrangement with the rest of the Ag nanowires used to stabilize the system. It is thus of practical importance to be able to use Ag capped SiNW arrays as high SERS substrates. In the results shown in Fig. 13, the more rigid and shorter SiNWs produced using a shorter etching time enhances the SERS sensitivity due to interparticle-coupling-induced Raman enhancement [56–58]. On the contrary, gravity and van der Waals force cause bending of the longer SiNWs and agglomeration of the Ag caps, subsequently reducing the SERS intensity. Hence, Ag capped SiNW arrays fabricated using self-selective electroless plating has potential applications in SERS-based biosensors.

2.4. Properties and applications of dendrites

2.4.1. Highly surface-enhanced Raman scattering active substrates for molecular sensing

Since the discovery of surface-enhanced Raman spectroscopy in the mid 1970s, tremendous efforts have been spurred to design and fabricate highly SERS active substrates for molecular sensing [59–61]. So far, the most studied and best established SERS-active systems are substrates sprayed with Ag or Au colloids [62–64]. Though spraying Ag or Au colloids on a substrate leads to an extremely high SERS signal at some local "hot spots", it has not been easy to achieve a reliable, stable, and uniform SERS signal that spans a wide dynamic range using this method. This is because the isolated particles and closely packed crystal-like structures, which exhibit weak SERS enhancement, are components of the colloids. Except for small nanoparticles dimers and fractal aggregates, they can produce such "super-hot spots". The SERS effect has a predominantly electromagnetic origin, that is, due to an increase in the local optical field exciting the molecule and multiplicative amplification of the re-radiated Raman scattered light [64]. In small nanoparticle dimers and aggregates, the SERS enhancement is attributable to interparticle coupling and so the interstitial sites are the enhancing locations. Fractals do not possess translational invariance and therefore, they cannot transmit ordinary waves. Accordingly, dynamic excitation such as vibration tends to be localized in fractals. More importantly, interaction among particles in the fractal cluster leads to a redistribution of the plasmon amplitude from a large number of particles into a much larger amplitude localized on a few particles. It produces the giant local fields in subwavelength sized "hot spots" [65–71]. Localization of optical eigenmodes and the associated strong field fluctuations can also lead to a dramatic SERS in fractals.

Dendritic networks formed in self-selective electroless plating are natural large fractal aggregates which are supposed to be excellent SERS active substrates. Using rhodamine 6G as conventional probe molecules, silver dendrites grown on silicon wafers in aqueous HF solution, containing the appropriate amount of silver nitrate were detached and tested for SERS. The silver dendritic networks are shown to have a high SERS enhancement factor with a large dynamic range. It is also worth noting that the enhancing power is uniform on the entire sample. Furthermore, the enhancing power is comparable (within the same order of magnitude) for different batches of substrates prepared by the same processing parameters, indicating good overall uniformity and reliability of the silver dendritic networks. In comparison with SERS substrates produced from metallic colloids and roughened metal surfaces, the low variation in the enhanced Raman signal from various substrates further indicates that the molecular adsorption behavior and chemical Raman enhancement effect are relatively insensitive to the fabrication procedures. Hence, in conjunction with the uniformly large enhancement factor obtained across the entire silver dendritic networks, the large dynamic range (more than three orders of magnitude) renders self-selective electroless plating a good technique for plasmon-based analytical devices, especially SERS-based biosensors.

Similar work has been reported on gold dendritic networks as SERS substrates [72]. The SERS signals from the gold dendrite networks dispersed on the silicon surface using self-selective electroless plating demonstrate that the approach is suitable for the production of SERS active substrates with high stability that can be employed to detect low concentrations of target molecules and biomolecules such as DNA and proteins.

2.4.2. Superhydrophobic property

It has been reported that when a silicon wafer covered by the Ag dendritic network is further modified by a self-assembled monolayer of *n*-dodecanethiol, a superhydrophobic surface with a contact angle of about 154° and a tilt angle lower than 5° can be obtained [73]. This property may lead to a novel and facile method to fabricate self-cleaning coatings on silicon [74–77]. Such superhydrophobic coatings can be applied on silicon by separating the electrolyte from the electrode. It may lead to an efficient nanobattery with a high power density, long shelf life, instantaneous and fast ramping up to full power, scalability, and chemistry-independent functionality [78]. The facile self-selective electroless plating technique can be an alternative technique to produce stable super-hydrophobic coatings on a large scale. Similar properties have also been observed in gold dendritic networks after modification of the self-selective electroless plated gold films with *n*-dodecanethiol [79]. It is believed that the various gold micro-nanostructures that account for the large fraction of air in the gold coatings contribute to the super-hydrophobicity.

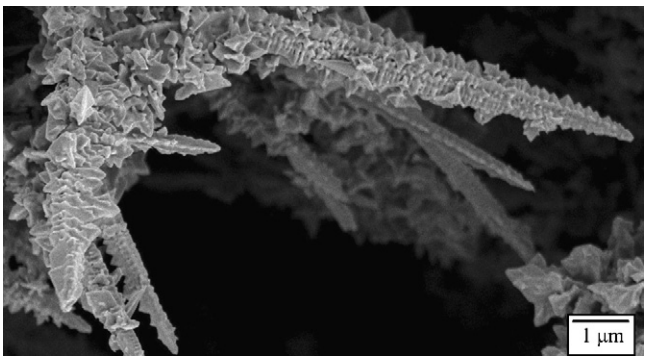

Fig. 14. SEM images of the whisker-like gold dendrites grown on silicon wafers via self-selective electroless plating in a 5.0 mol/L HF solution containing 0.02 mol/L $KAuCl_4$ at 50 °C. The etching time is 30 min. Reprinted with permission from ref. [83]. Copyright 2005 by American Institute of Physics.

2.4.3. Photoluminescence property

Photoluminescence (PL) from gold nanostructures is interesting from the viewpoint of electroluminescence devices in which semitransparent gold electrodes are used [80]. A good understanding of the optical processes in gold nanostructures is not only of fundamental interest but also reveals important information concerning applications in SERS, nonlinear optics, and surface-enhanced fluorescence [81,82]. By adopting the self-selective electroless plating technique, whisker-like gold dendrites shown in Fig. 14 have been fabricated [83]. A green PL band is observed at 550 nm and the emission peaks around 550 nm are centered near the interband absorption edge of bulk gold [84]. The enhanced PL from whisker-like gold dendrites relative to bulk gold is important to nano-optics. It is because optically excited metal surfaces exhibit no or very little luminescence. For instance, smooth gold films show PL with very a low efficiency of $\sim 10^{-10}$ following excitation of the electronic transition from 5d to 6sp bands [84]. In other words, only one photon is emitted by excitation of 10^{10} electron–hole pairs. One likely reason for this low PL efficiency is that the nonradiative energy relaxation processes of photoexcited carriers in metals such as Coulomb carrier–carrier scattering are much faster than radiative electron–hole recombination thus quenching PL [85]. We believe that the intensity enhancement observed for the green emission from the radiative recombination of sp-band electrons with d-band holes may be due to size-dependent screening effects which accelerate electron–electron scattering leading to emission by hot carriers of particle plasmons, that is, local electric field associated with the gold particle plasmons oscillations [86–88]. The exact origin of this effect is still controversial and remains a subject of investigation [85,89–91].

3. Self-selective electroless plating on Ge

Aizawa et al. have reported unique silver nanostructures—nano-inukshuks fabricated on germanium using self-selective electroless plating using only an aqueous $AgNO_3$ solution and Ge wafer [92]. The germanium–germanium bonds in the crystal lattice act as the reducing agent for the Ag^+ ions in the solution, leading to Ag(s) and concomitant oxidation of Ge(s) to Ge^{4+} in the spontaneous redox reaction. In contrast to reactions on silicon, the resulting Ge^{4+} product, germanium oxide, is water-soluble and does not form an insulating dielectric which inhibits further metal deposition in the absence of a fluoride source [93,94]. Fig. 15 shows an optical image of a 1 cm^2 germanium wafer and SEM images acquired from different regions. The nano-inukshuks form on most of the wafer except the middle area. It is believed that the wafer orientation is relatively unimportant for nano-inukshuk formation as they are observed on both Ge(1 1 1) and Ge(1 0 0) as well as the rough edges of germanium. Doping, either n- or p-type, affects the deposition rate during self-selective electroless plating. The Volmer–Weber mechanism has been proposed to explain the formation of these unique silver nanostructures [94]. However, the evolvement of the germanium wafers during self-selective electroless plating has not been monitored in details. In spite of two SEM images showing the etched germanium in Fig. 16, there are still questions about why the nanoholes form, why the silver nanostructures grow in the holes, and what the final pattern of the etched germanium wafers should be. Thus, further investigation should focus on the pattern evolvement of the germanium wafers and it is our belief that germanium nanowire arrays can be fabricated eventually.

4. Functional 1D composite nanomaterials fabricated using self-selective electroless plating

4.1. Oriented large-area Si nanowire p–n junction diode arrays

Self-selective electroless plating can be used to fabricate large-area oriented SiNW p–n junction diodes and superlattice arrays when using planar silicon p–n junction and superlattice wafers as the starting materials instead of n-type or p-type silicon wafers [95]. Fig. 17 shows the procedure used to fabricate large-area SiNW p–n junction diode arrays. The protocol is similar to that used to prepare SiNW arrays. The difference is that the starting materials are planar silicon p–n junction wafers and the thickness of the n-type silicon film is 9 μm. After immersion of the planar p–n junction wafers in an aqueous HF solution containing the appropriate amount of silver nitrate, at 50 °C, large-area oriented SiNW p–n junction diode arrays can quickly assemble on the surface of the silicon wafer due to highly self-selective process. The etched planar silicon p–n junction wafers are covered by a layer of thick silver dendritic film which is normal in self-selective electroless plating and can be easily detached from the surface.

Using current-sensing atomic force microscopy (AFM), the current versus voltage curves of the SiNW p–n diode bundles at various locations on the substrate can be readily investigated. The preliminary results disclose a nonlinear and rectifying behavior, perhaps due to the SiNW p–n diode. However, further analysis shows that the rectifying behavior can also arise from a Schottky diode rather than the nanowire p–n diode because the silver nanoparticles remaining on the nanowires render rectifying metal semiconductor contacts. Nevertheless, by means of self-selective electroless plating, the electrical properties of the SiNW p–n junctions can be tailored because the electrical properties of the planar silicon p–n junctions can be pre-established. Direct and predictable synthesis of SiNW p–n junction diode arrays represents an important step towards the fabrication of SiNW-based nanodevices [96–99]. In particular, this technique provides large-scale production of SiNW-based nanodevices at low costs. In addition, the oriented large-area SiNW p–n junction diode arrays have potential applications in optoelectronics and energy fields.

4.2. Organic and inorganic p–n heterojunction arrays

Inspired by the approach to fabricate SiNW p–n junction diode arrays [95], Cheng et al. have prepared p-poly(9,9-diethylfluorene) (PDEF)/n-SiNW heterojunctions by spin coating p-type conductive organic polymer on as-prepared n-SiNWs fabricated by self-selective electroless plating [100]. The schematic illustration of the fabrication process for a p-PDEF/n-SiNW heterojunction is depicted in Fig. 18. Organic-inorganic hybrid systems at the nanometer scale have attracted considerable attention due to the fast charge transfer rates between high electron affinity inorganic semiconductors and relatively low ionization potential organic

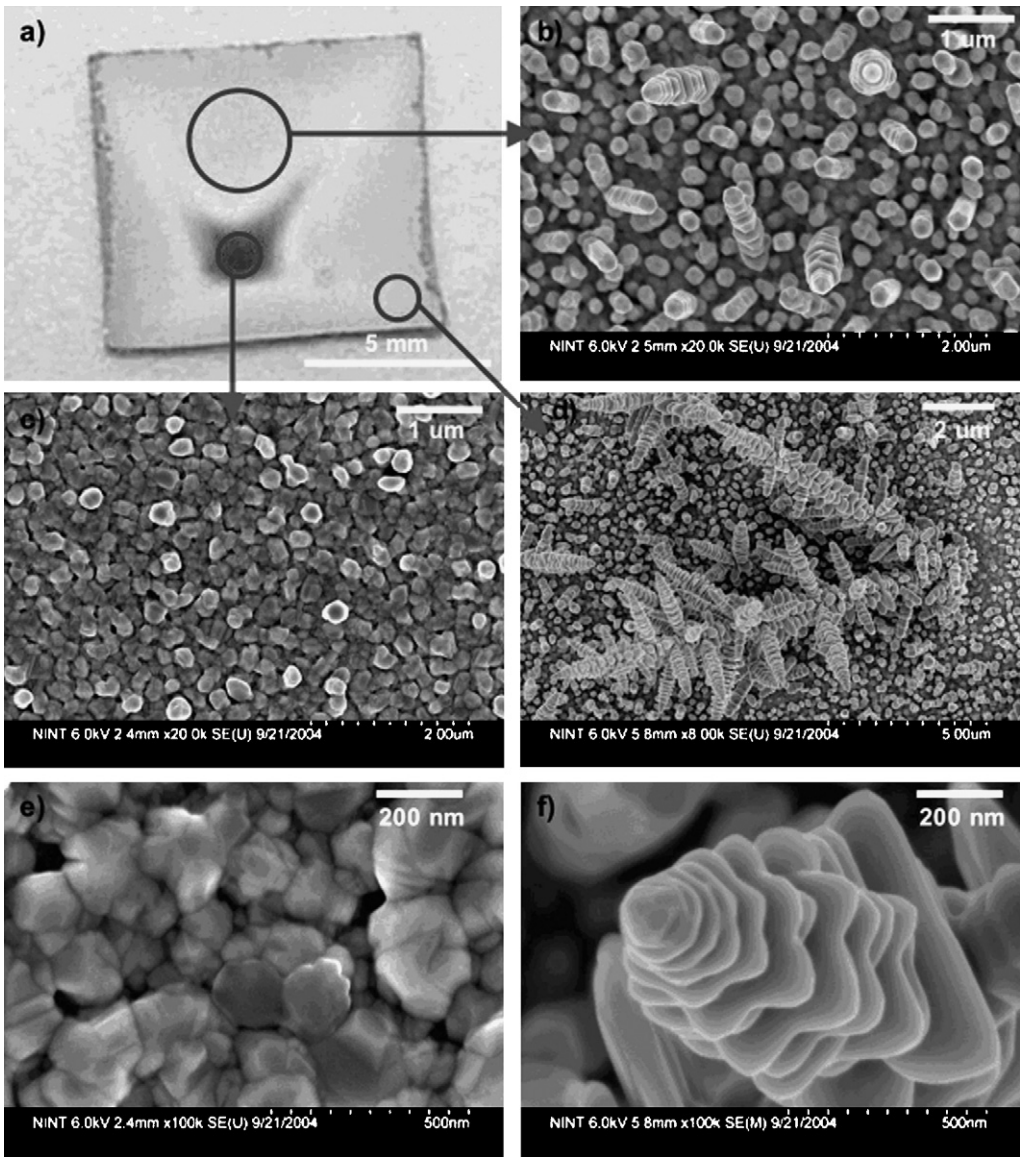

Fig. 15. Demonstration of different regions of silver deposition across the face of a Ge(1 0 0) n-type wafer after 4 h in 1.0×10^{-3} mol/L $AgNO_3$: (a) optical photograph of a 1 cm diameter wafer, showing the X-shape and areas of silver deposition, (b) aligned nano-inukshuks form predominately on the flat planes across the front of the wafer, as shown in this SEM, (c and e) SEM images of the center of the X-shape; EDS indicates that this central area is made up of germanium oxide and some silver, (d and f) toward the corners, dendritic structures are observed (SEM images). Reprinted with permission from ref. [92]. Copyright 2005 by American Chemical Society.

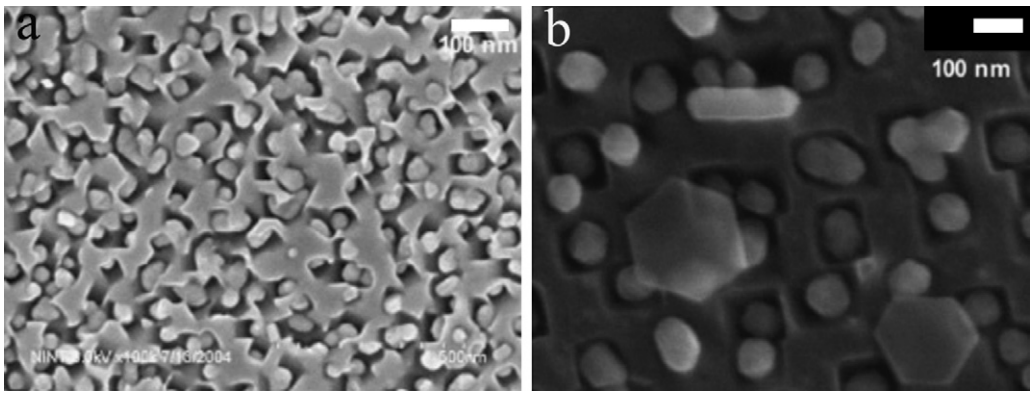

Fig. 16. 1.0×10^{-4} mol/L silver nitrate deposition conditions, demonstrating local etching of the germanium substrate induced by silver nanoparticle formation on the surface: (a) p-type Ge(1 1 1) after 1 h deposition and (b) p-type Ge(1 0 0) following 5 h of deposition. Reprinted with permission from ref. [92]. Copyright 2005 by American Chemical Society.

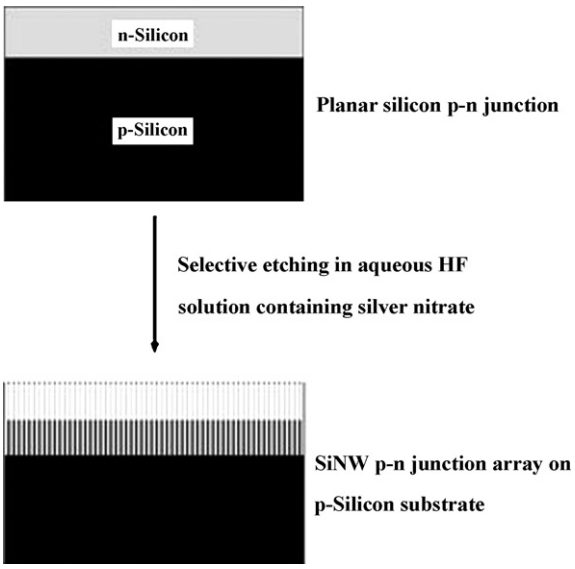

Fig. 17. Schematic illustration of the preparation of SiNW p–n junction diode arrays. Reprinted with permission from ref. [95]. Copyright 2004 by WILEY-VCH Verlag GmbH & Co. KGaA, Weinheim.

molecules [101–103]. Organic–inorganic hybrid systems have also been applied to flat panel displays [104]. The main advantage of such hybrid devices is the possibility of altering the composition of the organic film to effect large changes in its optical and electronic properties. In addition, the high injection current with quantum effect at nano-sized junctions formed by crossing p- and n-type nanowires indicates that high performance devices can be developed by employing nanowires in the structures. Hence, the p-PDEF/n-SiNW heterojunction structure is expected to have high efficiency by improving the carrier injection efficiency through the nano-sized junctions.

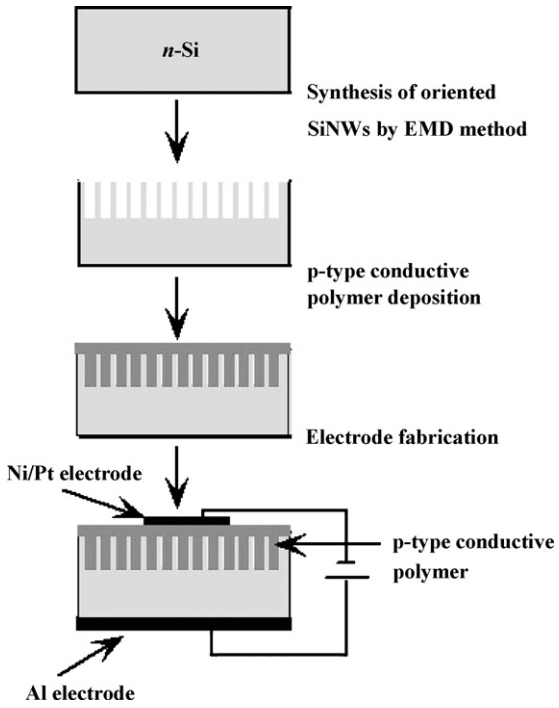

Fig. 18. Schematic illustration of the fabrication process for a p-PDEF/n-SiNW heterojunction. Reprinted with permission from ref. [100]. Copyright 2007 by American Institute of Physics.

The electrical properties of p-PDEF/n-SiNW heterojunctions have been investigated by using temperature-dependent and light-intensity-dependent *I–V* measurements. The data demonstrate good rectifying behavior with large reverse breakdown voltage and high rectification ratio. A response of 3.23 mA/W at a reverse bias of 10 V and the good photovoltaic properties are suitable for potential applications to future nanoelectronic and photonic devices.

4.3. Nanobeacons: Si nanowires with alterable visible light-emitting caps

Since the discovery of porous silicon with visible emission at room temperature [47], the light-emitting properties of Si-based semiconductor nanomaterials such as Si quantum dots [105,106], Si/SiO_x [107,108], and SiNWs [109,110] have attracted considerable attention and been investigated widely. A distinctive feature of Si nanostructured materials compared to the bulk counterpart is the well-known quantum confinement effect attributable to the reduced size and/or dimensionality [110,111]. In order to obtain blue emission from SiNWs via the quantum confinement effect so as to widen their applications in modern optoelectronics, the nanowire diameters must be reduced to several nanometers [112–114]. Many methods such as vapor–liquid–solid, solid–liquid–solid, and oxide-assisted growth have hitherto been proposed to synthesize SiNWs and their optical properties have been studied as well [115–121]. Most of the PL results show green to red emission and only a few reports describe blue emission arising from oxygen-related defects in SiNWs [110,122,123]. This is because the existence of oxygen can lead to the formation of some oxygen-related electronic states and thus weaken the quantum confinement effect. Since it is quite difficult to fabricate blue emitting SiNWs with good control, it may be better to assemble visible light-emitting semiconductor nanomaterials at the tips of SiNWs. This process has been demonstrated using self-selective electroless plating on silicon wafers covered with luminescent materials as the starting substrate [124].

Fig. 19 displays the schematic diagram of the formation process of SiO_xN_y-capped SiNW arrays. A silicon wafer covered with a 150 nm thick α-SiO_xN_y thin films is treated by plasma immersion ion implantation and deposition (PIII&D) [125,126]. Since the α-SiO_xN_y layer is reactive to HF, the SiO_xN_y-capped SiNWs are formed by self-selective electroless plating. Although it has been reported that α-SiO_xN_y thin films exhibit blue emission at 440 nm due to the recombination of holes and electrons in localized states corresponding to Si–N bonds (this is the reason why the starting materials are chosen [127,128]), an enhanced blue PL band is observed from the SiO_xN_y-capped SiNWs. Emission and excitation spectral analyses suggest that generation of photo-excited carriers takes place mainly in the quantum confined SiNWs, whereas their radiative recombination occurs in the Si–N binding states of the

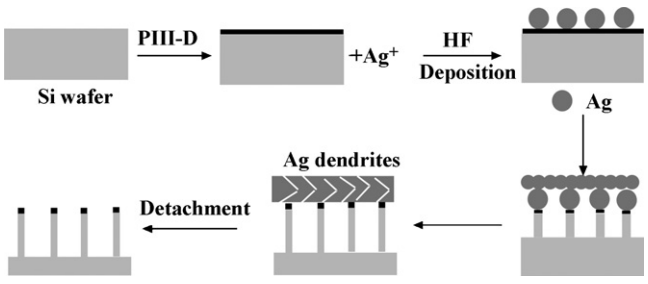

Fig. 19. Schematic illustration of the growth process of the SiO_xN_y-capped SiNW arrays. Reprinted with permission from ref. [124]. Copyright 2005 by American Institute of Physics.

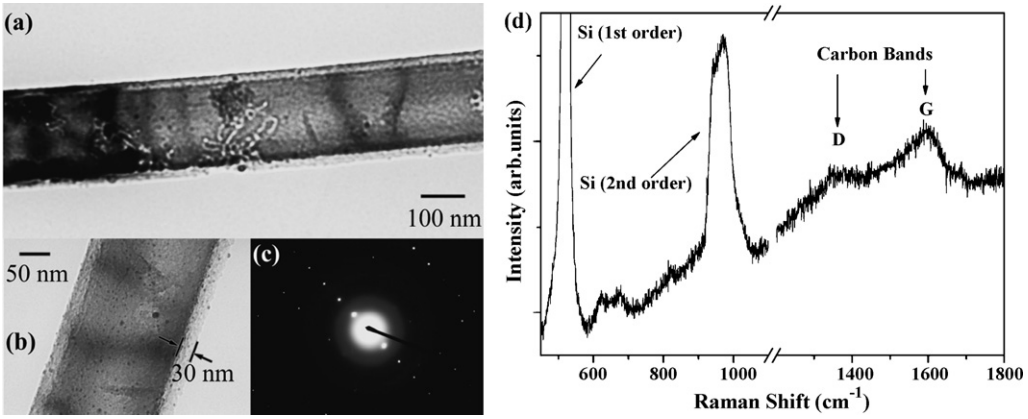

Fig. 20. (a) TEM image of a composite SiNW. (b) High-resolution TEM image of another composite SiNW. (c) The selected area diffraction pattern of the composite nanowire shown in (b). (d) Raman spectrum from the composite Si nanostructures. Reprinted with permission from ref. [30]. Copyright 2006 by American Vacuum Society.

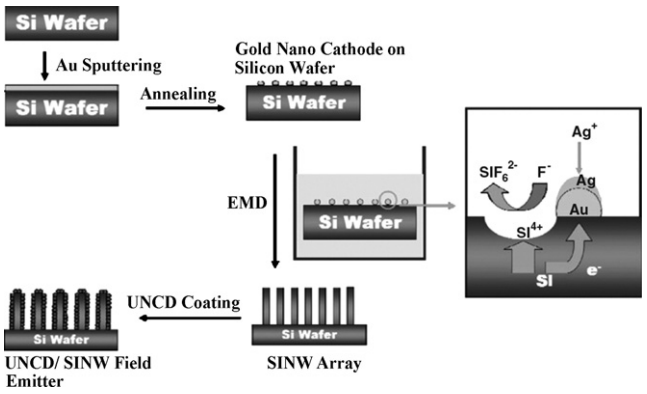

Fig. 21. Preparation procedure of the UNCD/SiNW field emitters. Reprinted with permission from ref. [135]. Copyright 2007 by IOP Publishing Ltd.

SiO_xN_y nanocaps. Therefore, the optical properties of SiNWs based luminescent composite produced by self-selective electroless plating can be tailored because the optical properties of the luminescent cover layers can be pre-established.

Simplified procedures resulting from the production of special oxygen-related defects on the top of SiNWs have also been reported [129]. In crystalline SiO_2, absorption of photons with energy higher than the band gap generates electron–hole pairs and a substantial proportion of them are converted to excitons. These excitons become self-trapped excitons when localized by self-induced lattice distortion due to the strong electron–phonon interaction, accompanied by defect formation and structural changes [130]. The radiative recombination of self-trapped excitons can produce a blue PL band at 460 nm [131]. Using water as the source of oxygen in PIII&D in order to achieve a smaller spread in the oxygen implant profile, SiO_x films with self-trapped excitons can be produced on the silicon wafer. After treatment in aqueous HF solution containing the appropriate amount of silver nitrate at 50 °C, large-area oriented SiO_x-capped SiNW arrays with strong blue emission can be readily and easily produced by self-selective electroless plating.

4.4. Si nanowires with sheaths

Semiconductor nanowires need to have an inorganic passivation layer because an unprotected surface may alter their optical and electrical properties [111]. A versatile method in which composite SiNW structures with diamond-like carbon sheaths act as the inorganic passivation layers has been proposed using plasma technology [30]. Fig. 20 shows a long SiNW sheathed with a thin diamond-like carbon film and the corresponding Raman spectrum acquired from the nanostructures. The diameter (~200 nm) of the coated SiNWs is relatively uniform. Using Beer's law to quantify the thickness of the thin Raman active coatings on the Raman active substrates, the thickness of the current diamond-like carbon

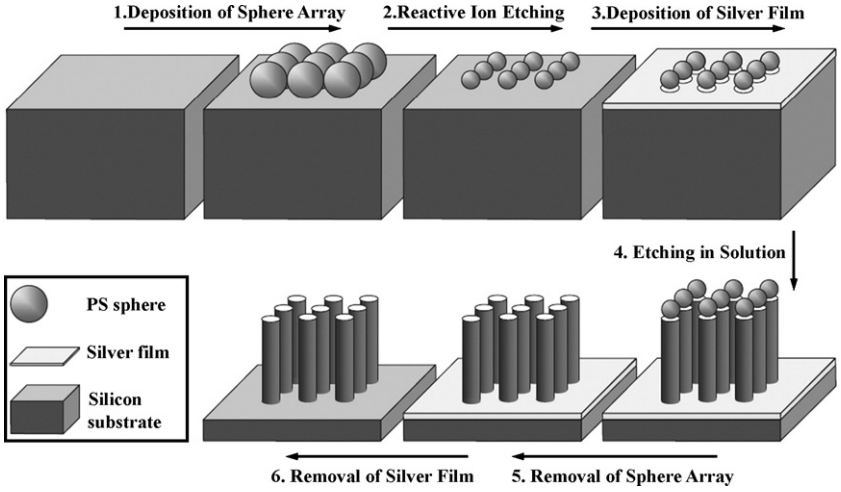

Fig. 22. Schematic depiction of the fabrication process of SiNW arrays with controlled diameter, length and diameter. Reprinted with permission from ref. [136]. Copyright 2007 by WILEY-VCH Verlag GmbH & Co. KGaA, Weinheim.

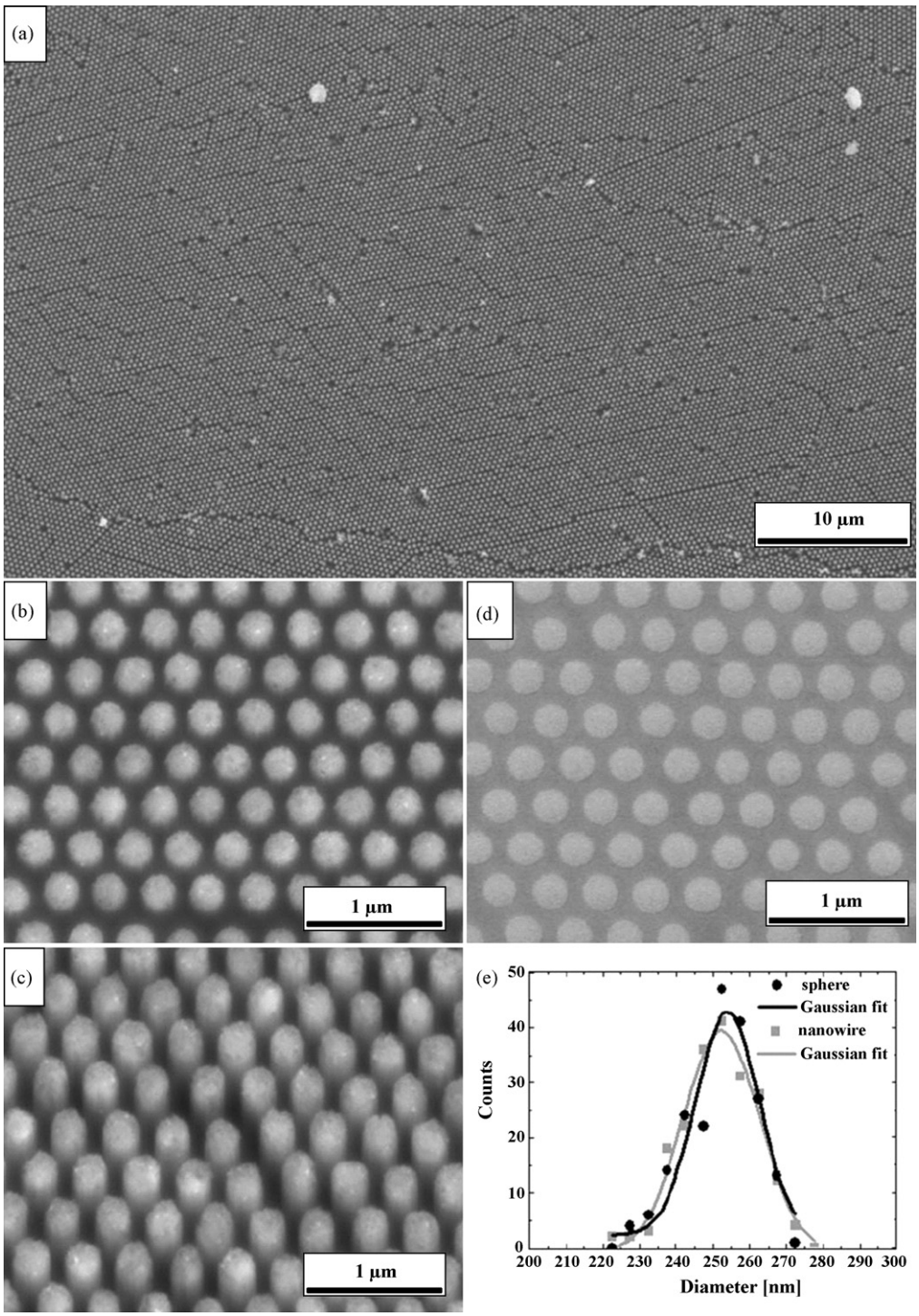

Fig. 23. SEM images of SiNW arrays: (a) low-magnification image, high magnification (b) plane-view and (c) tilted-view (ca. 15°) images, (d) SEM image of the polystyrene template used to grow the nanowires, (e) size distribution of SiNWs and diameter-reduced polystyrene spheres. Reprinted with permission from ref. [136]. Copyright 2007 by WILEY-VCH Verlag GmbH & Co. KGaA, Weinheim.

coating layer is calculated to be less than 50 nm [132–134] which is in good agreement with the TEM result. Hence, self-selective electroless plating has been experimentally shown to produce uniform SiNW arrays with passivation layers.

Tzeng et al. have exploited the superior properties of ultra-nanocrystalline diamond (UNCD) with an array of SiNWs to enhance the electron field-emission behavior [135]. The UNCD/SiNW field emitters are prepared by microwave plasma-enhanced chemical vapor deposition (PECVD) of UNCD on SiNW arrays with tunable diameters. The preparation procedures are illustrated in Fig. 21. The SiNW arrays are prepared by self-selective electroless plating in a $HF/AgNO_3$ solution on silicon wafers uniformly coated with gold particles. A thin layer of UNCD is coated on the SiNWs using microwave PECVD producing the UNCD/SiNW field-emitter arrays. It is shown that coating the SiNWs with a thin layer of UNCD film further improves the electron field emission properties of the materials. The threshold field to attain $J_e = 0.1$ mA/cm^2 electron field-emission current density decreases from 16.0 V/μm from

bare SiNWs to 10.2 V/μm from UNCD/SiNWs. In comparison, the electron field emission current density at an applied field of 15 V/μm increases from about 0.1 mA/cm^2 from the bare SiNWs to larger than 7.0 mA/cm^2 from the UNCD/SiNWs. The effective work functions of field emission are 0.0203 and 0.0160 eV for bare SiNWs and UNCD/SiNWs, respectively. The lower work function of the UNCD materials compared to that of silicon may be the main factor improving the electron field emission properties of the materials.

5. Controlled growth of Si nanowire arrays

Although self-selective electroless plating has been successfully applied to the fabrication of SiNWs with uniform crystallographic orientation, this process does not allow reliable control pertaining to the location and size of the nanowires. Recently, Huang et al. have reported modifications to the self-selective electroless plating technique in order to fabricate SiNWs with precisely controlled diameter, length and density [136]. Fig. 22 demonstrates the fabrication process. Initially, the template consisting of a monolayer of polystyrene spheres is allowed to self-assemble on a Si substrate. A reactive ion etching process is then used to reduce the diameter of the polystyrene spheres. It leads to the formation of colloidal particle arrays that are no longer closely packed. In the next step, a silver film is thermally evaporated onto the silicon substrate as a catalyst. Owing to the polystyrene monolayer mask, a silver film with a hexagonal array of holes is formed. The diameter of the holes matches that of the diameter-reduced polystyrene spheres. Subsequently, an etching step is conducted in a mixture of deionized water, HF, and H_2O_2. The Ag film catalyzes etching of silicon beneath it. During the etching process, the "walls" of the honeycomb are gradually etched away and the remnant silicon forms a nanowire array. Finally, the polystyrene spheres are removed by dissolution in $CHCl_3$ and the Ag film is dissolved in boiling aqua regia.

Compared to usual self-selective electroless plating in which Ag dendrites randomly form on the silicon, the characteristic features of the modified technique is that the sinking of Ag etches the silicon and only the silicon beneath the designed pattern of the Ag layer can be catalytically etched. The mean diameter of the nanowires using this self-selective electroless plating method matches the corresponding value of the diameter-reduced polystyrene spheres as shown in Fig. 23. The diameter of the SiNWs can be controlled by selecting polystyrene spheres with the desired reduced diameter leading to different center-to-center distances between the nanowires. This implies that the center-to-center distance between the nanowires (or the density of the nanowire arrays) can also be controlled by selecting polystyrene spheres of an appropriate original diameter. The length of the nanowires is observed to vary linearly with the duration of the etching process, thereby providing good control on the length of the nanowire arrays. All in all, the modified self-selective electroless plating technique allows precise control on the diameter, length, and density of the SiNWs.

6. Future challenges

Although substantial progress has been made with regard to the understanding the self-selective electroless plating, there are challenges in the roadmap before the technique can be used more extensively to fabricate functional 1D nanomaterials. Some of key issues are listed below:

(1) Growth mechanism—In self-selective electroless plating on Si, some people believe that Ag protects the silicon underneath from being etched [18,23–25,27], while some others postulate that Ag particles only catalyze etching of the Si substrate in contact with them [31,32]. Another school of thought is that the network structure of the Ag clusters affects the formation of perpendicular SiNWs [33]. However, these proposed mechanisms are not backed up by sufficient experimental evidence and some presumptions must be made. Thus, investigation of the detailed mechanism of self-selective electroless plating on Si requires more research.

(2) Nanowires synthesis—Though controlled synthesis of SiNW arrays by self-selective electroless plating has been developed, it is premature to generalize the approach to produce a variety of semiconductor nanowires. For example, in self-selective electroless plating on Ge, intermediate nanoholes are found on the surface of the etched germanium wafers [92]. Subsequent chemical dissolution of the thin pore walls is believed to enlarge the pores and lead to merging of adjacent pores. Hence, after a sufficiently long etching time, a high density of nanowires should remain on the surface [29,30]. However, very little attention has been paid to the evolution of the germanium wafers during self-selective electroless plating. We believe that self-selective electroless plating may also be extended to other materials such as SiC and GaN. Hence, there is an immediate need not only to investigate the characteristics of self-selective electroless plating on Si but also to find new applications and fabricate other semiconductor nanowires.

(3) Dendrites synthesis—Although the growth mechanism of silver/gold dendrites appears to be fairly well understood, there are remaining questions regarding the two noble metals. Generally, metal nanoclusters have strong tendency to coalesce and form a continuous film in electroless plating [23]. Electroless plating of Pt and Cu in HF normally can generally be categorized in this way. Since dendrite-like metal coatings play a crucial role in the formation of nanowire arrays and have potential applications in plasmon-based analytical devices [72], deeper investigation of the intrinsic characteristics of silver/gold dendrites is required.

(4) Functional nanomaterials—Nanotechnology is based upon the ability to create nanostructured materials that produce novel and unique properties. Although it is possible to produce prototype nanodevices such as SiNW-based photovoltaic cells [40], SiNW p–n junction diode arrays [95], and p-PDEF/n-SiNW heterojunctions [100] with the help of self-selective electroless plating, the technique must be extended and more ingenious engineering is needed for large scale production.

In conclusion, recent advances in self-selective electroless plating have been reviewed. Many functional 1D nanomaterials can be produced by this technique and the possible growth mechanisms and future challenges are discussed. The technique plays an important role in the development of novel and unique nanodevices that cannot otherwise be fabricated by traditional methods. It should be noted that research on self-selective electroless plating is still in the beginning stage and progress is needed for more widespread applications of this technique in nanotechnology.

Acknowledgements

The authors are grateful for the financial support from Scientific Research Fund of Southeast University for Talents Introduction (Grant No. 4007021024), City University of Hong Kong Strategic Research Grant (SRG) No. 7002138, and Hong Kong Research Grants Council (RGC) Competitive Earmarked Research Grant (CERG) No. 112307.

References

[1] A. Brenner, G.E. Riddell, Proc. Am. Electropl. Soc. 33 (1946) 4.
[2] A. Brenner, G.E. Riddell, Proc. Am. Electropl. Soc. 34 (1947) 156.
[3] H. Narcus, Met. Finish. 45 (1947) 64.
[4] A.E. Cahill, Proc. Am. Electropl. Soc. 44 (1957) 130.
[5] N. Khoperia, Microelectron. Eng. 69 (2003) 384.
[6] X. Li, P.W. Bohn, Appl. Phys. Lett. 77 (2000) 2572.
[7] X.L. Li, Y.W. Kim, P.W. Bohn, I. Adesida, Appl. Phys. Lett. 80 (2002) 980.
[8] T.L. Rittenhouse, P.W. Bohn, I. Adesida, Solid State Commun. 126 (2003) 245.
[9] H. Morinaga, M. Suyama, T. Ohmi, J. Electrochem. Soc. 141 (1994) 2834.
[10] J.S. Kim, H. Morita, J.D. Joo, T. Ohmi, J. Electrochem. Soc. 144 (1997) 3275.
[11] N. Mitsugi, K. Nagai, J. Electrochem. Soc. 151 (2004) G302.
[12] K. Tsujino, M. Matsumura, Electrochem. Solid State Lett. 8 (2005) C193.
[13] K. Tsujino, M. Matsumura, Adv. Mater. 17 (2005) 1045.
[14] R.B. Wehrspohn, J. Schilling, Phys. Status Solidi A 197 (2003) 673.
[15] S. Ottow, V. Lehmann, H. Föll, Appl. Phys. A: Mater. Sci. Process. 63 (1996) 153.
[16] S. Cruz, A. Hönig-d' Orville, J. Müller, J. Electrochem. Soc. 152 (2005) C418.
[17] S. Yae, Y. Kawamoto, H. Tanaka, N. Fukumuro, H. Matsuda, Electrochem. Commun. 5 (2003) 632.
[18] K.Q. Peng, Y.J. Yan, S.P. Gao, J. Zhu, Adv. Mater. 14 (2002) 1164.
[19] P. Gorostiza, J. Servat, J.R. Morante, F. Sanz, Thin Solid Films 275 (1996) 12.
[20] P. Gorostiza, R. Diaz, F. Sanz, J.R. Morante, J. Electrochem. Soc. 144 (1997) 4119.
[21] P. Gorostiza, R. Diaz, M.A. Kulandainathan, F. Sanz, J.R. Morante, J. Electroanal. Chem. 469 (1999) 48.
[22] P. Gorostiza, M.A. Kulandainathan, R. Diaz, F. Sanz, P. Allongue, J.R. Morante, J. Electrochem. Soc. 147 (2000) 1026.
[23] K.Q. Peng, Y.J. Yan, S.P. Gao, J. Zhu, Adv. Funct. Mater. 13 (2003) 127.
[24] K.Q. Peng, J. Zhu, Electrochim. Acta 49 (2004) 2563.
[25] T. Qiu, X.L. Wu, G.G. Siu, P.K. Chu, J. Electron. Mater. 35 (2006) 1879.
[26] W.P. Gomes, S. Lingier, D. Vanmaekelbergh, J. Electroanal. Chem. 269 (1989) 237.
[27] T. Qiu, X.L. Wu, X. Yang, G.S. Huang, Z.Y. Zhang, Appl. Phys. Lett. 84 (2004) 3867.
[28] T. Qiu, X.L. Wu, J.C. Shen, P.C.T. Ha, P.K. Chu, Nanotechnology 17 (2006) 5769.
[29] T. Qiu, X.L. Wu, Y.F. Mei, G.J. Wan, P.K. Chu, G.G. Siu, J. Cryst. Growth 277 (2005) 143.
[30] T. Qiu, X.L. Wu, L.W. Yang, P.N. Shen, Z.Y. Zhang, G.G. Siu, P.K. Chu, J. Vac. Sci. Technol. B 24 (2006) 1702.
[31] K.Q. Peng, J.J. Hu, Y.J. Yan, Y. Wu, H. Fang, Y. Xu, S.T. Lee, J. Zhu, Adv. Funct. Mater. 16 (2006) 387.
[32] K.Q. Peng, H. Fang, J.J. Hu, Y. Wu, J. Zhu, Y.J. Yan, S.T. Lee, Chem. Eur. J. 12 (2006) 7942.
[33] H. Fang, Y. Wu, J.H. Zhao, J. Zhu, Nanotechnology 17 (2006) 3768.
[34] P.H. Chang, G. Berman, C.C. Shen, J. Appl. Phys. 63 (1988) 1473.
[35] T.B. Massalski, H. Okamoto, P.R. Subramanian, L. Kacprzak, Binary Alloy Phase Diagram, 2nd edn, ASM International, Materials Park, OH, 1990.
[36] T.A. Witten Jr., L.M. Sander, Phys. Rev. Lett. 47 (1981) 1400.
[37] T. Qiu, X.L. Wu, Y.F. Mei, P.K. Chu, G.G. Siu, Appl. Phys. A: Mater. Sci. Process. 81 (2005) 669.
[38] J.P. Xiao, Y. Xie, R. Tang, M. Chen, X.B. Tian, Adv. Mater. 13 (2001) 1887.
[39] K.Q. Peng, Y. Wu, H. Fang, X.Y. Zhong, Y. Xu, J. Zhu, Angew. Chem. Int. Ed. 44 (2005) 2737.
[40] K.Q. Peng, Y. Xu, Y. Wu, Y.J. Yan, S.T. Lee, J. Zhu, Small 1 (2005) 1062.
[41] H. Seidel, L. Csepregi, A. Heuberger, H. Baumgartel, J. Electrochem. Soc. 137 (1990) 3612.
[42] U. Gangopadhyay, K.H. Kim, D. Mangalaraj, J.S. Yi, Appl. Surf. Sci. 230 (2004) 364.
[43] C. Levy-Clement, A. Lagoubi, M. Neumann-Spallart, M. Rodot, R. Tenne, J. Electrochem. Soc. 138 (1991) L69.
[44] M. Lipinski, P. Panek, E. Beltowska, H. Czternastek, Mat. Sci. Eng. B 101 (2003) 297.
[45] X.L. Wu, S.J. Xiong, G.G. Siu, G.S. Huang, Y.F. Mei, Z.Y. Zhang, S.S. Deng, C. Tan, Phys. Rev. Lett. 91 (2003) 157402.
[46] J. Sun, Y.W. Lu, X.W. Du, S.A. Kulinich, Appl. Phys. Lett. 86 (2005) 171905.
[47] L.T. Canham, Appl. Phys. Lett. 57 (1990) 1046.
[48] C.H. Chen, Y.F. Chen, Appl. Phys. Lett. 75 (1999) 2560.
[49] M. Sakurai, C. Thirstrup, M. Aono, Phys. Rev. B 62 (2000) 16167.
[50] C. Li, G.J. Fang, S. Sheng, Z.Q. Chen, J.B. Wang, S. Ma, X.Z. Zhao, Physica E 30 (2005) 169.
[51] Z. Iqbal, S. Veperk, J. Phys. C 15 (1982) 377.
[52] H. Richter, Z.P. Wang, L. Ley, Solid State Commun. 39 (1981) 625.
[53] I.H. Campbell, P.M. Fauchet, Solid State Commun. 58 (1986) 739.
[54] L. Tian, K.B. Ram, I. Ahmad, L. Menon, M. Holtz, J. Appl. Phys. 97 (2005) 026101.
[55] S.J. Lee, A.R. Morrill, M. Moskovits, J. Am. Chem. Soc. 128 (2006) 2200.
[56] F.J. García-Vidal, J.B. Pendry, Phys. Rev. Lett. 77 (1996) 1163.
[57] V.A. Markel, V.M. Shalaev, P. Zhang, W. Huynh, L. Tay, T.L. Haslett, M. Moskovits, Phys. Rev. B 59 (1999) 10903.
[58] M. Futamata, Y. Maruyama, M. Ishikawa, J. Phys. Chem. B 107 (2003) 7607.
[59] M. Fleischmann, P.J. Hendra, A.J. McQuillan, Chem. Phys. Lett. 26 (1974) 163.
[60] D.L. Jeanmaire, R.P. van Duyne, J. Electroanal. Chem. 84 (1977) 1.
[61] M.G. Albrecht, J.A. Creighton, J. Am. Chem. Soc. 99 (1977) 5215.
[62] K. Kneipp, Y. Wang, H. Kneipp, L.T. Perelman, I. Itzkan, R.R. Dasari, M.S. Feld, Phys. Rev. Lett. 78 (1996) 1667.
[63] S. Nie, S.R. Emory, Science 275 (1997) 1102.
[64] M. Moskovits, Rev. Mod. Phys. 57 (1985) 783.
[65] M.I. Stockman, L.N. Pandey, L.S. Muratov, T.F. George, Phys. Rev. Lett. 72 (1994) 2486.
[66] V.M. Shalaev, R. Botet, J. Mercer, E.B. Stechel, Phys. Rev. B 54 (1996) 8235.
[67] M.I. Stockman, Phys. Rev. E 56 (1997) 6494.
[68] V.M. Shalaev, A.K. Sarychev, Phys. Rev. B 57 (1998) 13265.
[69] S. Gresillon, L. Aigouy, A.C. Boccara, J.C. Rivoal, X. Quelin, C. Desmarest, P. Gadenne, V.A. Shubin, A.K. Sarychev, V.M. Shalaev, Phys. Rev. Lett. 82 (1999) 4520.
[70] V.M. Shalaev, M.I. Stockman, R. Botet, Physica A 185 (1992) 181.
[71] V.M. Shalaev, R. Botet, D.P. Tsai, J. Kovacs, M. Moskovits, Physica A 207 (1994) 197.
[72] C.H. Wang, D.C. Sun, X.H. Xia, Nanotechnology 17 (2006) 651.
[73] F. Shi, Y.Y. Song, J. Niu, X.H. Xia, Z.Q. Wang, X. Zhang, Chem. Mater. 18 (2006) 1365.
[74] R.E. Johnson, R.H. Dettre, Adv. Chem. Ser. 43 (1964) 12.
[75] W. Barthlott, C. Neinhuis, Planta 202 (1997) 1.
[76] L. Feng, S.H. Li, Y.S. Li, H.J. Li, L.J. Zhang, J. Zhai, L.Y. Song, B.Q. Liu, L. Jiang, D.B. Zhu, Adv. Mater. 14 (2002) 1857.
[77] T.L. Sun, L. Feng, X.F. Gao, L. Jiang, Acc. Chem. Res. 38 (2005) 644.
[78] V.A. Lifton, S. Simon, R.E. Frahm, Bell Labs Tech. J. 10 (2005) 81.
[79] C.H. Wang, Y.Y. Song, J.W. Zhao, X.H. Xia, Surf. Sci. 600 (2006) L38.
[80] Z. Gaburro, G. Pucker, P. Belluti, L. Pavesi, Solid State Commun. 114 (2000) 33.
[81] R.G. Ispasiou, L. Balogh, O.P. Varnavski, D.A. Tomalia, T. Goodson III, J. Am. Chem. Soc. 122 (2000) 11005.
[82] A. Wokaum, H.D. Lutz, A.P. King, U.P. Wild, R.R. Ernst, J. Chem. Phys. 79 (1983) 509.
[83] T. Qiu, X.L. Wu, G.G. Siu, P.K. Chu, Appl. Phys. Lett. 87 (2005) 223115.
[84] A. Mooradian, Phys. Rev. Lett. 22 (1969) 185.
[85] E. Dulkeith, T. Niedereichholz, T.A. Klar, J. Feldmann, G. von Plessen, D.I. Gittins, K.S. Mayya, F. Caruso, Phys. Rev. B 70 (2004) 205424.
[86] C. Voisin, D. Christofilos, N. Del Fatti, F. Vallée, B. Prével, E. Cottancin, J. Lermé, M. Pellarin, M. Broyer, Phys. Rev. Lett. 85 (2000) 2200.
[87] T.V. Shahbazyan, I.E. Perakis, J.-Y. Bigot, Phys. Rev. Lett. 81 (1998) 3120.
[88] T.V. Shahbazyan, I.E. Perakis, Chem. Phys. 251 (2000) 37.
[89] M.B. Mohamed, V. Volkov, S. Link, M.A. El-Sayed, Chem. Phys. Lett. 317 (2000) 517.
[90] G.T. Boyd, Z.H. Yu, Y.R. Shen, Phys. Rev. B 33 (1986) 7923.
[91] O.P. Varnavski, M.B. Mohamed, M.A. El-Sayed, T. Goodson III, J. Phys. Chem. B 107 (2003) 3101.
[92] M. Aizawa, A.M. Cooper, M. Malac, J.M. Buriak, Nano Lett. 5 (2005) 815.
[93] L. Magagnin, R. Maboudian, C. Carraro, J. Phys. Chem. B 106 (2002) 401.
[94] L.A. Porter Jr., H.C. Choi, A.E. Ribbe, J.M. Buriak, Nano Lett. 2 (2002) 1067.
[95] K.Q. Peng, Z.P. Huang, J. Zhu, Adv. Mater. 16 (2004) 73.
[96] Y. Cui, Q. Wei, H. Park, C.M. Lieber, Science 293 (2001) 1289.
[97] X. Duan, Y. Huang, Y. Cui, J.F. Wang, C.M. Lieber, Nature 409 (2001) 66.
[98] Y. Huang, X. Duan, Y. Cui, L. Lauhon, K.H. Kim, C.M. Lieber, Science 294 (2001) 1313.
[99] M.S. Gudiksen, L.J. Lauhon, J. Wang, D.C. Smith, C.M. Lieber, Nature 415 (2002) 617.
[100] Y.Z. Cheng, G.J. Fang, C. Li, L.Y. Yuan, L. Ai, B.R. Chen, X.Z. Zhao, Z.Y. Chen, W.B. Bai, C.M. Zhan, J. Appl. Phys. 102 (2007) 083516.
[101] N.C. Greenham, X.G. Peng, A.P. Alivisatos, Phys. Rev. B 54 (1996) 17628.
[102] D.S. Ginger, N.C. Greenham, Phys. Rev. B 59 (1999) 10622.
[103] J.M. Rehm, G.L. McLendon, Y. Nagasawa, K. Yoshihara, J. Moser, M. Gratzel, J. Phys. Chem. 100 (1996) 9577.
[104] C. Qu, Z. Xu, F. Tang, L. Qian, W.G. Yu, S.Y. Shan, X.R. Xu, Chin. Phys. Lett. 21 (2004) 552.
[105] M.V. Wolkin, J. Jorne, P.M. Fauchet, Phys. Rev. Lett. 82 (1999) 197.
[106] T. Qiu, X.L. Wu, F. Kong, H.B. Ma, P.K. Chu, Phys. Lett. A 334 (2005) 447.
[107] Y. Kanemitsu, T. Ogawa, K. Shiraishi, K. Takeda, Phys. Rev. B 48 (1993) 4883.
[108] T.V. Torchynska, A.D. Cano, M.M. Rodriguez, L.Y. Khomenkova, Physica B 340 (2003) 1113.
[109] J. Qi, J.M. White, A.M. Belcher, Y. Masumoto, Chem. Phys. Lett. 372 (2003) 763.
[110] S. Bhattacharya, D. Banerjee, K.W. Adu, S. Samui, S. Bhattacharyya, Appl. Phys. Lett. 85 (2004) 2008.
[111] A.P. Alivisators, Science 271 (1996) 933.
[112] Y.F. Zhang, Y.H. Tang, N. Wang, D.P. Yu, C.S. Lee, I. Bello, S.T. Lee, Appl. Phys. Lett. 72 (1998) 1835.
[113] A.M. Morales, C.M. Lieber, Science 279 (1998) 208.
[114] D.D.D. Ma, C.S. Lee, F.C.K. Au, S.Y. Tong, S.T. Lee, Science 299 (2003) 1874.
[115] J.L. Gole, J.D. Stout, W.L. Rauch, Z.L. Wang, Appl. Phys. Lett. 76 (2000) 2346.
[116] H.F. Yan, Y.J. Xing, Q.L. Hang, D.P. Yu, Y.P. Wang, J. Xu, Z.H. Xi, S.Q. Feng, Chem. Phys. Lett. 323 (2000) 224.
[117] D.P. Yu, Y.J. Xing, Q.L. Hang, H.F. Yan, J. Xu, Z.H. Xi, S.Q. Feng, Physica E 9 (2001) 305.
[118] X.H. Sun, N.B. Wong, C.P. Li, S.T. Lee, J. Appl. Phys. 96 (2004) 3447.
[119] S.T. Lee, Y.F. Zhang, N. Wang, Y.H. Tang, I. Bello, C.S. Lee, Y.W. Chung, J. Mater. Res. 14 (1999) 4503.
[120] J.F. Qi, J.M. White, A.M. Belcher, Y. Masumoto, Chem. Phys. Lett. 372 (2003) 763.
[121] J.F. Qi, A.M. Belcher, J.M. White, Appl. Phys. Lett. 82 (2003) 2616.
[122] D.D.D. Ma, S.T. Lee, J. Shinar, Appl. Phys. Lett. 87 (2005) 033107.
[123] A.R. Guichard, D.N. Barsic, S. Sharma, T.I. Kamins, M.L. Brongersma, Nano Lett. 6 (2006) 2140.
[124] T. Qiu, X.L. Wu, G.J. Wan, Y.F. Mei, G.G. Siu, P.K. Chu, Appl. Phys. Lett. 86 (2005) 193111.

[125] P.K. Chu, B.Y. Tang, Y.C. Cheng, P.K. Ko, Rev. Sci. Instrum. 68 (1997) 1866.
[126] P.K. Chu, S. Qin, C. Chan, N.W. Cheung, L.A. Larson, Mat. Sci. Eng. R 17 (1996) 207.
[127] T. Noma, K.S. Seol, H. Kato, M. Fujimaki, Y. Ohki, Appl. Phys. Lett. 79 (2001) 1995.
[128] C. Ance, F.D. Chelle, J.P. Ferraton, G. Leveque, P. Ordejon, F. Yndurain, Appl. Phys. Lett. 60 (1992) 1399.
[129] T. Qiu, X.L. Wu, Y.T. Xie, Y.F. Mei, G.G. Siu, P.K. Chu, Nanotechnology 16 (2005) 2222.
[130] C. Itoh, K. Tanimura, N. Itoh, J. Phys. C 21 (1988) 4693.
[131] C. Itoh, T. Suzuki, N. Itoh, Phys. Rev. B 41 (1989) 3794.
[132] N. Gopinathan, C. Robinson, F. Ryan, Thin Solid Films 355 (1999) 401.
[133] H. Kohira, F.E. Talke, J. Tribol. 122 (2000) 288.
[134] T.W. Scharf, I.L. Singer, Thin Solid Films 440 (2003) 471.
[135] Y.F. Tzeng, K.H. Liu, Y.C. Lee, S.J. Lin, I.N. Lin, C.Y. Lee, H.T. Chiu, Nanotechnology 18 (2007) 435703.
[136] Z.P. Huang, H. Fang, J. Zhu, Adv. Mater. 19 (2007) 744.